KAERI/TR-3177/2006

Development of PARA-ID Code to Simulate Inelastic Constitutive Equations and Their Parameter Identifications for the Next Generation Reactor Designs

Korea Atomic Energy Research Institute

제 출 문

한국원자력연구소소장 귀하

본 보고서를 “Development of PARA-ID Code to Simulate Inelastic Constitutive Equations and Their Parameter Identifications for the Next Generation Reactor Designs,”에 대한 기술보고서로 제출합니다.

2006 년 3 월 27 일

연 구 기 관 명 : 한국원자력연구소

과 제 명 : 액체금속로 기계설계 기술개발

주 저 자 : 구 경 회

공 동 저 자 : 이 재 한

요 약 문

차세대 원자로 설계를 위해서는 고온 비탄성해석 기술의 확보가 필수적이다. 본 보고서에서는 주어진 설계재료에 대한 라체칭, 크립-피로손상 해석에 필수적인 비탄성 구성방정식을 개발하기 위하여 지금까지 개발된 구성식 들의 특성을 검토하고 이들 구성식에 들어가는 재료상수들을 결정하기 위한 방법론을 확립하였다. 이를 위하여 각 구성방정식에 대한 Simulation 코드인 PARA-ID (PARAmeter-IDentification) 프로그램을 개발하고 이로부터 각 구성식에 요구되는 재료상수를 결정할 수 있는 절차를 정립하였다.

ABSTRACT

The establishment of the inelastic analysis technology is essential issue for a development of the next generation reactors subjected to elevated temperature operations. In this report, the peer investigation of constitutive equations in points of a ratcheting and creep-fatigue analysis is carried out and the methods extracting the constitutive parameters from experimental data are established. To perform simulations for each constitutive model, the PARA-ID (PARAmeter-IDentification) computer program is developed. By using this code, various simulations related with the parameter identification of the constitutive models are carried out.

LISTS OF CONTENTS

Abstract ---------- **2**

LISTS OF CONTENTS ---------- **3**

1. Introduction ---------- **5**

2. Constitutive Equations for Ratcheting Models ---------- **6**

2.1 Theoretical Formulation of Plasticity ---------- **7**

2.1.1 Yield Condition ---------- **7**

2.1.2 Plastic Flow Rule ---------- **10**

2.1.3 Hardening Rule ---------- **11**

2.2 Cyclic Plasticity Constitutive Models ---------- **12**

2.2.1 Linear and Multilinear Kinematic Hardening Model ---------- **12**

2.2.2 Nonlinear Armstrong and Frederick Model ---------- **13**

2.2.2.1 Constitutive Equations

2.2.2.2 Elasto-Plastic Modulus

2.2.2.3 Cyclic Behavior

2.2.2.4 Parameter Identification

2.2.3 Chaboche 3-Decomposed Model ---------- **21**

2.2.3.1 Constitutive Equations

2.2.3.2 Cyclic Behavior

2.2.3.3 Parameter Identification

2.2.4 Chaboche Model with A Threshold ---------- **33**

2.2.4.1 Constitutive Equations

2.2.4.2 Cyclic Behavior

2.2.4.3 Parameter Identification

2.2.5 Ohno and Wang Model ---------- **37**

2.2.5.1 Constitutive Equations

2.2.5.2 Cyclic Behavior

2.2.5.3 Parameter Identification

2.3 Comparison Study ---------- 41

2.3.1 Stress-Controlled Behavior ---------- 41

2.3.2 Strain-Controlled Behavior ---------- 42

2.3.3 Ratcheting Behavior ---------- 44

3. Cyclic Viscoplasticity Constitutive Model ---------- 45

3.1 Unified Chaboche Model ---------- 45

3.2 Examples of Application ---------- 46

4. PARA-ID Code ---------- 52

4.1 Salient Features of PARA-ID ---------- 52

4.2 General Procedures ---------- 52

4.3 Input Commands and Formats ---------- 52

5. Conclusions ---------- 58

Acknowledgement ---------- 58

Nomenclature ---------- 58

Reference ---------- 60

Bibliographic Information Sheet ---------- 63

1. Introduction

In most LMR (Liquid Metal Reactor) designs, the operating temperature is very high at over 500^{o}C and the design lifetime is designed for much more than 30 years. Therefore, a time-dependent creep rupture, excessive creep deformation, cyclic creep ratcheting, creep-fatigue, creep crack growth and a creep buckling become very important for a reactor structural design. Unlike with conventional PWR, the normal operating conditions can be basically dominant design loading because the hold time at an elevated temperature condition is enough long to result in severe creep damage during total service lifetime. For the purpose of the high temperature structural integrity evaluation in design of nuclear power plants, the worldwide design codes and assessment procedures such as ASME-NH(USA), RCC-MR(France), R5(UK), and DDS(Japan) are developed or under development status.

To make substantial engineering design rules, most of the evaluation rules contained in the design codes are based on the elastic analysis method, which is using the elastic stress and strain calculation results. However these methods may be very conservative in some design conditions, therefore the structural integrities can not be satisfied in some critical points of the components and equipments. To overcome the conservatism contained in the elastic analysis method and make a satisfaction of the reactor structural design the inelastic analysis methods are inevitably required to be introduced in the elevated temperature reactor design process. In using the inelastic analysis method there are couples of issues to be resolved in actual design stages such as selections of the inelastic constitutive models, determinations of the load histories, significant engineering costs which will be a computing time for the load history of a whole design lifetime, and so on. Among these issues, the selection of the inelastic constitutive models involves big issues of the identification of the material parameters associated with their equations.

In this study, the various constitutive equations for ratcheting simulation are investigated and programmed to be used to identify the equation parameters. Many researchers have made the efforts in developing constitutive models for ratcheting:

- Linear Kinematic Hardening

(Prager, 1956)

- Multilinear Model
  (Mroz, 1967)
- Nonlimear Kinematic Hardening
  (Armstrong and Frederick, 1966, Guionnet, 1992)
- Decomposed Nonlinear Kinematic Hardening
  (Chaboche, 1979, 1986)
- Decomposed Nonlinear Kinematicv Hardening with Threshold
  (Chaboche, 1991; Ohno and Wang, 1993)
- Modified Chaboche(1991) or Ohno and Wang(1993) Model
  (McDowell, 1995) (Jiang and Sehitoglu, 1996)
  (Voyiadjis and Basuroychowdhury, 1998)
  (AbdelKarim and Ohno, 2000)
  (Bari and Hassan, 2001, 2002)

To obtain the material parameters contained in the constitutive models, the PARA-ID (PARAmeter-IDentification) computer program is developed. With using this code, the cyclic behaviors of the material are characterized and comparison of each model is carried out.

Finally, to be able to perform the simulation of the time-dependent material behavior due to the viscous effects, the unified Chaboche viscoplastic model is reviewed and implemented in PARA-ID code. The viscous effects invoking the stress relaxation, creep strain increment, and the strain rate dependent hardening behavior are investigated by the simulation with the material parameters of 316L used by Chaboche (1989).

2. Constitutive Equations for Ratcheting Models

According to the ASME-NH design rules, the definition of a ratcheting is a progressive cyclic inelastic deformation. Describing it in more detail, a ratcheting is the accumulation of the plastic strain cycle-by-cycle for a certain stress amplitude with a non-zero mean stress. Most metals reveal cyclic hardening or softening behaviors to a

certain number of cycles and subsequently stabilize or cease to change the size of the yield surface. However, in some conditions mentioned above for the ratcheting descriptions, an inelastic strain keeps on occurring with cycles even after the material is stabilized. During this behavior, the translation of the yield surface in a stress space (kinematic hardening) is the dominant reason for a progressive incremental inelastic deformation.

As an isotropic hardening (i.e. yield surface size change) behavior stabilizes or ceases after a certain number of cycles, all of the ratcheting constitutive parameter identification are related with the kinematic hardening parameters and should be determined by using experiments performed on stabilized materials.

2.1 Theoretical Formulation of Plasticity

To formulate the plastic behavior of a work-hardening or softening material, it is required to use an initial yield condition, a plastic flow rule, and a hardening rule. An initial yield condition has a function to specify the state of a stress for which a plasticity will first occur. A plastic flow rule provides the magnitude of the plastic strain increment tensor and it defines its direction in the strain space. The hardening rule modifies the yield condition in the direction of the plastic flow.

2.1.1 Yield Condition

The yield condition is represented by a convex surface in the stress space. Assuming *f* as a yield function which depends on a complete previous stress and strain history of a material, the yield condition occurs whenever the loading function $F(\sigma_{ij})$ becomes equal to the constant *f* as follows;

$$F(\sigma_{ij}) = f \tag{1}$$

As shown in Fig. 1, when the loading increment *dF* is in the following condition (plastic loading),

$$dF = \frac{\partial F}{\partial \sigma_{ij}} \dot{\sigma}_{ij} > 0 \tag{2}$$

the state of a stress is moving out from the yield surface and a plastic behavior occurs. When the loading increment *dF* is zero (neutral loading) as in

$$dF = \frac{\partial F}{\partial \sigma_{ij}} \dot{\sigma}_{ij} = 0\,, \tag{3}$$

the state of a stress is moving on the yield surface.
Finally, when the loading increment *dF* is in the following condition (elastic loading),

$$dF = \frac{\partial F}{\partial \sigma_{ij}} \dot{\sigma}_{ij} < 0\,, \tag{4}$$

i.e., unloading condition, the state of a stress is moving in from the yield surface and going back to the elastic behavior.

Actually, it is well-known that the constitutive equations for the mechanical behavior of materials are generally based on the thermodynamical concepts [Chaboche, 1983]. In this study, a typical von Mises yield criteria, which is based on the thermodynamic forces associated with the two internal state variables such as the kinematic (back stress, α_{ij}) and the isotropic hardening (drag stress, *R*) variables, is used as follows;

$$f(\sigma_{ij} - a_{ij}) = \sqrt{\frac{3}{2}(\tau_{ij} - \alpha_{ij})(\tau_{ij} - \alpha_{ij})} - \sigma_{yo} - R = 0 \tag{5}$$

where σ_{ij} are the Cauchy stress tensor, a_{ij} are the total backstress tensor, τ_{ij} are the deviatoric stress tensor of the stress tensor σ_{ij} , α_{ij} is the deviatoric backstress tensor (the current center of the yield surface), σ_{yo} is the initial yield stress, and *R* is the isotropic hardening variable.

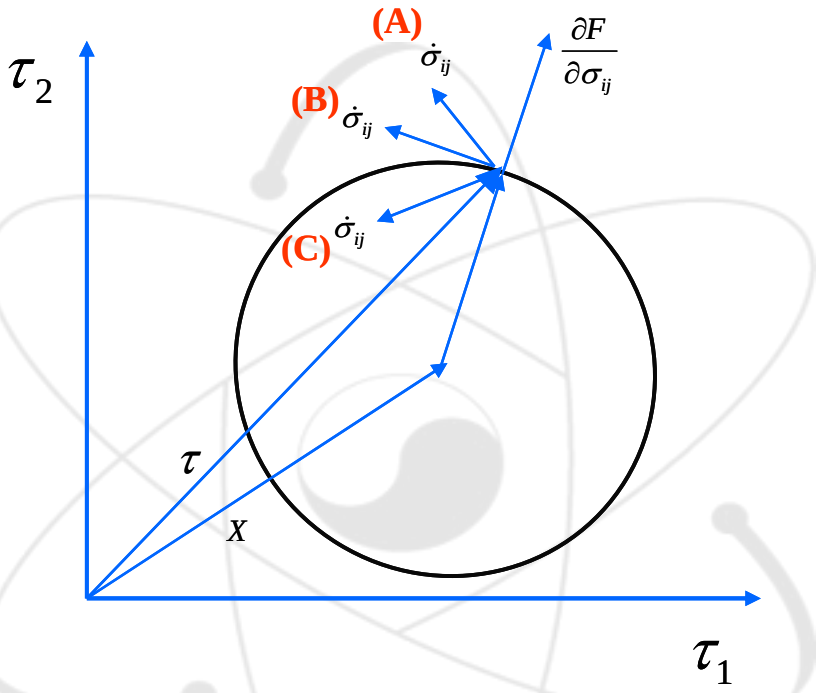

Fig. 1 Concept of Yield Surface Conditions

2.1.2 Plastic Flow Rule

The total strain increment tensor is the sum of the elastic and plastic strain increment tensors as follows;

$$\dot{\varepsilon}_{ij} = \dot{\varepsilon}_{ij}^{e} + \dot{\varepsilon}_{ij}^{p} \tag{6}$$

From the equation, the elastic strain can be easily obtained by differentiating the elastic potential function with respect to stress tensor σ_{ij}. Similarly, the plastic flow equations can be obtained with the plastic potential function g(σ_{ij}), which is a scalar function of the stresses as follows;

$$\dot{\varepsilon}_{ij}^{p} = \lambda \frac{\partial g}{\partial \sigma_{ij}} \tag{7}$$

where λ is a positive scale factor of a proportionality, which is zero in the elastic domain, and it is actually derived as

$$\lambda = \frac{1}{H} \left\langle \frac{\partial f}{\partial \sigma_{ij}} \bullet \dot{\sigma}_{ij} \right\rangle \tag{8}$$

where H is the plastic modulus, <> indicates the MacCauley bracket, and the symbol $\bullet$ presents the inner product as $\mathbf{a} \bullet \mathbf{b} = a_{ij} b_{ij}$. As shown in Eq. (7), the plastic flow vector $\dot{\varepsilon}_{ij}^{p}$ is directed along the normal to the surface of the plastic potential. For most stable materials, the flow rule is associative, i.e., the plastic potential function and the yield function coincide, $g = f$. In this case, the plastic flow rule is represented as

$$\dot{\varepsilon}_{ij}^{p} = \lambda \frac{\partial f}{\partial \sigma_{ij}} \tag{9}$$

and it develops along the normal direction to the yield surface.

2.1.3 Hardening Rule

When the state of a stress is over the elastic limit and the loading continues, a material hardening behavior can occur with one of two types or both. One is a kinematic hardening accounting for the yield surface translation in the deviatoric stress space. The other one is an isotropic hardening accounting for the expansion of the yield surface without its translation.

The most important feature for ratcheting simulation is the kinematic hardening rule. This rule will be investigated in detail in the next sections for various constitutive models.

Isotropic hardening model used in this study is represented as by Chaboche (1991) with the expression

$$\dot{R} = b[Q - R]\,\dot{p} \tag{10}$$

where b and Q are material parameters and $\dot{p}$ is the evolution of the accumulated plastic strain, which can be expressed as

$$\dot{p} = \sqrt{\frac{2}{3}\dot{\varepsilon}_{ij}^{p}\,\dot{\varepsilon}_{ij}^{p}} \tag{11}$$

When the initial value $R = 0$, integrating the Eq. (9) gives:

$$R = Q(1 - e^{-bp}) \tag{12}$$

According to the evolution of an isotropic hardening by Chaboche (1989) the material parameter Q can be represented as

$$Q = Q_M + (Q_0 - Q_M)\,e^{-2\mu q} \tag{13}$$

where Q_M , Q_0 , and μ are material parameters and q = $\left\| \dot{\varepsilon}_{ij}^{p} / 2 \right\|$.

Considering the time recovery effects, Chaboche has proposed an isotropic hardening model (1989) as

$$\dot{R} = b[Q - R]\,\dot{p} + \gamma_r \left| Q_r - R \right|^m sign(Q_r - R) \tag{14}$$

where

$$Q_r = Q - Q_r^* \left[1 - \left(\frac{Q_M - Q}{Q_M} \right)^2 \right] \tag{15}$$

2.2 Cyclic Plasticity Constitutive Models

2.2.1 Linear and Multilinear Kinematic Hardening Model

Prager (1956) has proposed the simplest kinematic hardening rule to simulate the plastic behavior of materials as follows;

$$\dot{\alpha}_{ij} = C\dot{\varepsilon}_{ij}^{p} \tag{16}$$

In this model, the yield surface moves linearly with the plastic strain as shown in the trace of the backstress (a_x) of Fig. 2 and the hysteresis loop is bilinear. Therefore, this model can not represent the nonlinear part of the hysteresis loop. Furthermore, this model only produces a closed hysteresis loop for a prescribed uniaxial stress cycle with a mean stress and it can not simulate the ratcheting behavior.

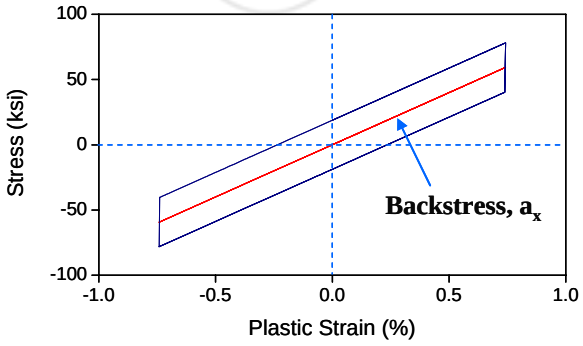

Fig. 2 Hysteresis Loop by the Prager Model

To improve the linear kinematic hardening model, many authors like Mroz (1967), Besseling (1958), Ohno and Wang, etc, have proposed the multilinear models. All these models are based on dividing the stress and strain curve into many linear segments. Actually these models shows a very good agreement in the nonlinear part of the hysteresis loop but they still provides a closed loop for a uniaxial stress cycle with a mean stress and can not simulate the uniaxial ratcheting behavior.

2.2.2 Nonlinear Armstrong and Frederick Model

2.2.2.1 Constitutive Equations

Armstrong and Frederick (1966) have proposed a nonlinear kinematic hardening model, which can describe the nonlinear parts of the hysteresis loop with a memory effect of the strain path.

The kinematic hardening rule in this model is represented with the evolution of the deviatoric backstress as follows;

$$\dot{\alpha}_{ij} = \frac{2}{3} C \dot{\varepsilon}_{ij}^{p} - \gamma \alpha_{ij} \dot{p} \tag{17}$$

In above equation, $\dot{p}$ is the evolution of the accumulated plastic strain expressed as

$$\dot{p} = \left| \dot{\varepsilon}_{ij}^{p} \right| = \left[\frac{2}{3} \dot{\varepsilon}_{ij}^{p} \dot{\varepsilon}_{ij}^{p} \right]^{1/2} \tag{18}$$

2.2.2.2 Plastic Modulus

As shown in the equation of the plastic strain evolution from the flow rule of Eq. (9), the simulation for a uniaxial ratcheting primarily depends on the plastic modulus calculation scheme. In this study, ratcheting is referred to as “uniaxial ratcheting for uniaxial loading”.

Most of the nonlinear kinemtaic hardening models are called a coupled model because the plastic modulus calculation is coupled with the kinematic hardening rule

through a consistency condition. After applying the consistency condition to the yield criterion of Eq. (5), the evolution of the yield function can be obtained as

$$\dot{f} \equiv \frac{\partial f}{\partial \tau_{ij}} \dot{\tau}_{ij} + \frac{\partial f}{\partial \alpha_{ij}} \dot{\alpha}_{ij} + \frac{\partial f}{\partial R} \dot{R} = 0 \tag{19}$$

Each derivative term can be obtained after differentiating the yield function with respect to the deviatoric stress as follows;

$$\frac{\partial f}{\partial \tau_{ij}} = \frac{3(\tau_{ij} - \alpha_{ij})}{2\sqrt{\frac{3}{2}(\tau_{ij} - \alpha_{ij})(\tau_{ij} - \alpha_{ij})}} \tag{20}$$

$$\frac{\partial f}{\partial \alpha_{ij}} = -\frac{\partial f}{\partial \tau_{ij}} \tag{21}$$

$$\frac{\partial f}{\partial R} = -1 \tag{22}$$

After substituting Eq.(20) – Eq.(22) into Eq.(19), one can obtain

$$\frac{\partial f}{\partial \tau_{ij}} (\dot{\tau}_{ij} - \dot{\alpha}_{ij}) - \dot{R} = 0 \tag{23}$$

The elasticity relationship between the Cauchy stress and strain tensor is defined as

$$\dot{\sigma}_{ij} = E_{ijkl} \dot{\varepsilon}^{e}_{kl} = E_{ijkl} (\dot{\varepsilon}_{kl} - \dot{\varepsilon}^{p}_{kl}) \tag{24}$$

where E_{ijkl} is the forth-order elastic modulus tensor. Substituting Eq.(17) and Eq.(24) into Eq.(23) one can obtain the equation as

$$\frac{\partial f}{\partial \sigma_{ij}}\left[E_{ijkl}(\dot{\varepsilon}_{kl} - \dot{\varepsilon}_{kl}^{p}) - \left(\frac{2}{3} C \dot{\varepsilon}_{ij}^{p} - \gamma \alpha_{ij} \dot{p}\right)\right] - b(Q-R)\dot{p} = 0 \tag{25}$$

where

$$\dot{p} = \left|\dot{\varepsilon}_{ij}^{p}\right| = \left[\frac{2}{3}\dot{\varepsilon}_{ij}^{p}\dot{\varepsilon}_{ij}^{p}\right]^{1/2} = \lambda\left[\frac{2}{3}\frac{\partial f}{\partial \sigma_{ij}}\frac{\partial f}{\partial \sigma_{ij}}\right]^{1/2} \tag{26}$$

After substituting Eq.(9) and Eq.(26) into Eq.(25), one can obtain

$$\frac{\partial f}{\partial \sigma_{ij}}\left[E_{ijkl}\dot{\varepsilon}_{kl} - E\lambda\frac{\partial f}{\partial \sigma_{kl}} - \frac{2}{3}C\lambda\frac{\partial f}{\partial \sigma_{ij}} + \gamma\alpha_{ij}\lambda\sqrt{\frac{2}{3}\frac{\partial f}{\partial \sigma_{ij}}\frac{\partial f}{\partial \sigma_{ij}}}\right] - b(Q-R)\lambda\sqrt{\frac{2}{3}\frac{\partial f}{\partial \sigma_{mn}}\frac{\partial f}{\partial \sigma_{mn}}} = 0 \tag{27}$$

After some arrangement in terms of $\dot{\varepsilon}_{ij}$ and λ, the following equation can be obtained.

$$\lambda\left(E_{ijkl}\frac{\partial f}{\partial \sigma_{ij}}\frac{\partial f}{\partial \sigma_{kl}} + \frac{2}{3}C\frac{\partial f}{\partial \sigma_{ij}}\frac{\partial f}{\partial \sigma_{ij}} - \gamma\frac{\partial f}{\partial \sigma_{ij}}\alpha_{ij}\sqrt{\frac{2}{3}\frac{\partial f}{\partial \sigma_{ij}}\frac{\partial f}{\partial \sigma_{ij}}} + b(Q-R)\sqrt{\frac{2}{3}\frac{\partial f}{\partial \sigma_{mn}}\frac{\partial f}{\partial \sigma_{mn}}}\right) = \dot{\varepsilon}_{kl}E_{ijkl}\frac{\partial f}{\partial \sigma_{ij}} \tag{28}$$

From Eq.(28) the positive scale factor can be expressed as

$$\lambda = \frac{1}{H}\frac{\partial f}{\partial \sigma_{ij}}E_{ijkl}\dot{\varepsilon}_{kl} \tag{29}$$

where *H* is defined as a plastic modulus,

$$H = E_{ijkl}\frac{\partial f}{\partial \sigma_{ij}}\frac{\partial f}{\partial \sigma_{kl}} + \frac{2}{3}C\frac{\partial f}{\partial \sigma_{ij}}\frac{\partial f}{\partial \sigma_{ij}} - \gamma\frac{\partial f}{\partial \sigma_{ij}}\alpha_{ij}\sqrt{\frac{2}{3}\frac{\partial f}{\partial \sigma_{ij}}\frac{\partial f}{\partial \sigma_{ij}}} + b(Q-R)\sqrt{\frac{2}{3}\frac{\partial f}{\partial \sigma_{mn}}\frac{\partial f}{\partial \sigma_{mn}}} \tag{30}$$

Substituting Eq.(9) and (29) into Eq.(24) one can obtain the equation as

$$\begin{aligned}\dot{\sigma}_{ij} &= E_{ijkl}\left(\dot{\varepsilon}_{kl} - \lambda\frac{\partial f}{\partial \sigma_{kl}}\right) \\ &= \left(E_{ijkl} - \frac{1}{H}E_{ijkl}\frac{\partial f}{\partial \sigma_{ij}}E_{ijkl}\frac{\partial f}{\partial \sigma_{kl}}\right)\dot{\varepsilon}_{kl}\end{aligned} \tag{31}$$

Eq.(31) can be rewritten as

$$\dot{\sigma}_{ij} = D_{ijkl}\dot{\varepsilon}_{kl} \tag{32}$$

where the elasto-plastic modulus tensor is defined as

$$D_{ijkl} = E_{ijkl} - \frac{1}{H}E_{ijkl}\frac{\partial f}{\partial \sigma_{ij}}E_{ijkl}\frac{\partial f}{\partial \sigma_{kl}} \tag{33}$$

2.2.2.3 Cyclic Behavior

The material parameters used in this example of a cyclic loading are taken from the published SPCEN mild steel [Puso, 2000] as

Kinematic Hardening : C = 23.7 GPa, γ = 416
Isotropic Hardening : Q = 37.7 MPa, b = 67.8
Yield Stress : σ_{yo} = 108 MPa
Young's Modulus : E = 153 GPa

By using the given parameters, theoretically the saturation stress should be

$$\begin{aligned}\sigma_{saturation} &= \sigma_{yo} + \frac{C}{\gamma} + Q \\ &= 108 + 23{,}700/416 + 37.7 \\ &= 202.67\,MPa\end{aligned} \tag{34}$$

Fig. 3 shows the stress-controlled stress-strain hysteresis loop for the steadily increasing loads at each loading cycle.

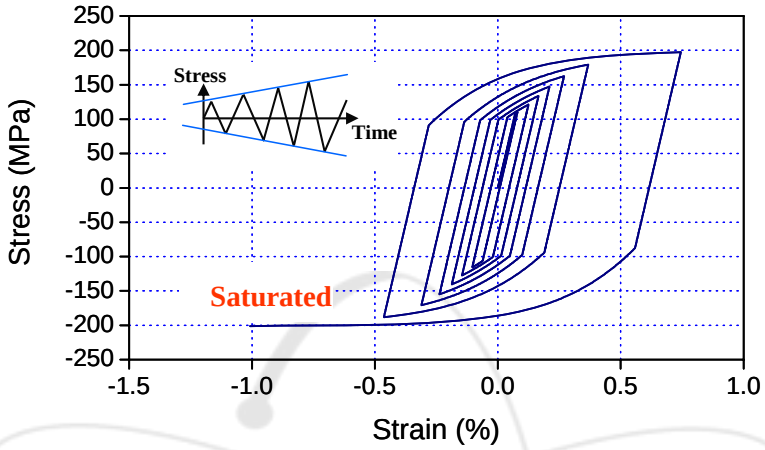

Fig. 3 Stress-Controlled Hysteresis Loop by the AF Model

As shown in figure, we can see that the loop is saturated at the theoretical value of the saturation stress as increasing the load amplitude. Fig. 4 shows the strain-controlled stress-plastic strain hysteresis loop and we can see that the maximum stress is exactly saturated at 202.67 MPa. When the load amplitude is so larger than the saturation stress level, then the yield surface translates and the hysteresis loop occur at large strain region as shown in Fig. 5.

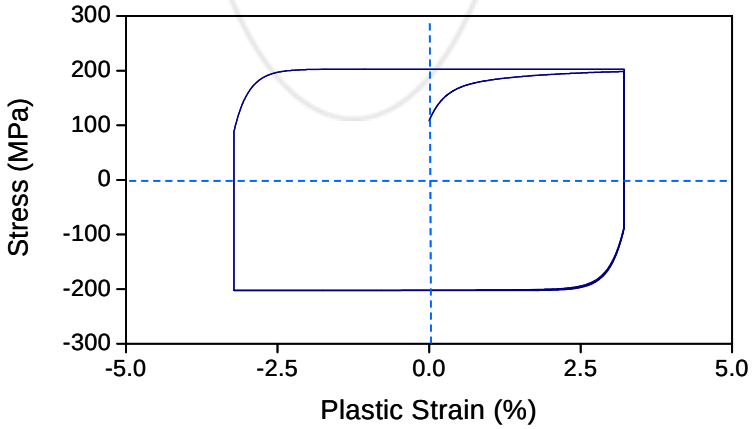

Fig. 4 Strain-Controlled Hysteresis Loop by the AF Model

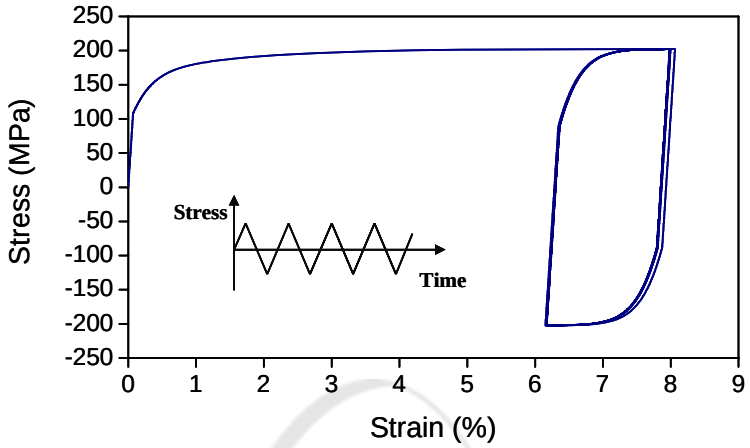

Fig. 5 Cyclic Behavior in Case of Large Load Magnitude

To investigate the characteristics of the material parameters of C and γ, the sensitivity studies are carried out. Fig. 6 shows the effects of a kinematic hardening parameter C with a constant value of γ by the stress-controlled simulations. As shown in the figure, by increasing the value of C, the material behavior after yielding becomes stiffer and the calculated strains become smaller. Fig. 7 shows the effects of the parameter γ with a constant value of C by the stress-controlled simulations. As shown in the figure, by increasing the value of γ, the material behavior after yielding becomes less stiff and the strain increases. For a uniaxial loading, the trace of a backstress a_x stabilizes to a value of C/γ after increasing some amount of plastic strain.

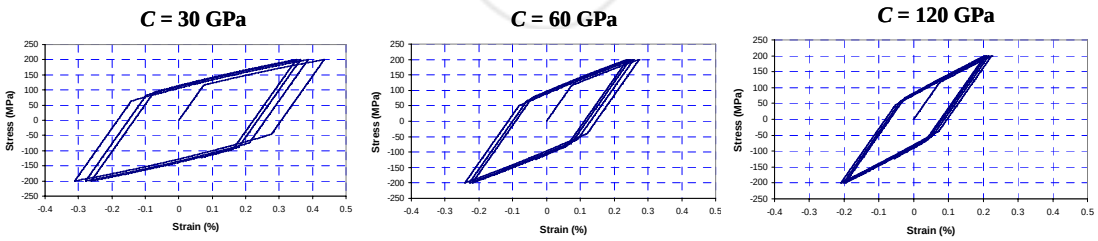

Fig. 6 Effects of Parameter C on Hysteresis Loop

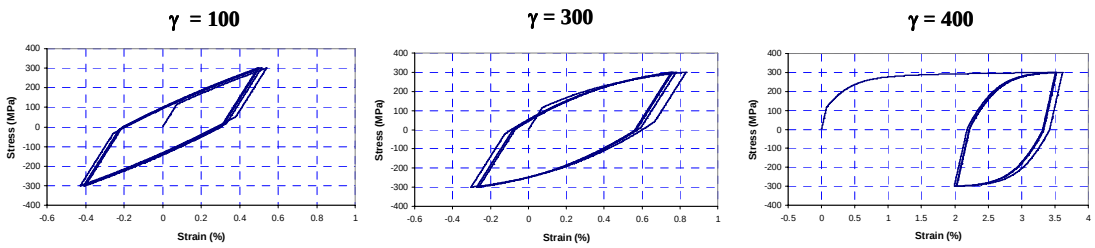

Fig. 7 Effects of Parameter γ on Hysteresis Loop

2.2.2.4 Parameter Identification

Identification of the material parameters associated with their material models is one of the most important issues, especially in field of a high temperature reactor structural design.

The identification procedure to obtain the material parameters C and γ contained in a backstress evolution equation is based on available experimental results. Substantially, as this model has just two parameters, there is no way to extract the adequate control parameter related with ratcheting behavior. Therefore, the stress-strain data obtained from the half cycle of the uniaxial tension or compression experiments is enough to extract the material parameters. Due to this reason, this approach is not adequate when the simulation involves large number of cyclic loadings with a mean stress, which can invoke ratcheting behavior.

Integrating the backstress evolution equation of Eq.(17) over a half cycle of a stress-strain experimental data, one can obtain the following expression

$$\alpha = S + (\alpha_0 - S)e^{-\gamma(\varepsilon^p - \varepsilon_0^p)} \tag{35}$$

where

$$S = \frac{2}{3}\frac{C}{\gamma} \tag{36}$$

In Eq. (35), the state of $(\dot{\varepsilon}_o^p, \alpha_o)$ results from the plastic flow.

In this study, the least-square error fitting method is used to extract the parameter C and γ from the finite set of experimental data points. In applying this method, Eq.(35) is not adequate form, therefore it is necessary to transform Eq.(35) into a form of the linear equation. To do this, we can rearrange the Eq.(35) as

$$\ln\left(\frac{S-\alpha_0}{S-\alpha}\right)=\gamma(\varepsilon^p-\varepsilon_0^p) \tag{37}$$

With assumption of the saturation stress (Fig. 8) at a point of no backstress evolution, i.e., $\dot{\alpha}=0$, the backstress is expressed as

$$\alpha=\alpha_s=S=\frac{2}{3}\frac{C}{\gamma} \tag{38}$$

Substituting Eq.(38) into Eq.(37), Eq.(37) can be rewritten as

$$\ln\left(\frac{\alpha_s-\alpha_0}{\alpha_s-\alpha}\right)=\gamma(\varepsilon^p-\varepsilon_0^p) \tag{39}$$

Therefore, Eq.(39) has a form of the linear equation as

$$Y=AX \tag{40}$$

where

$$Y=\ln\left(\frac{\alpha_s-\alpha_0}{\alpha_s-\alpha}\right),\quad A=\gamma,\quad X=(\varepsilon^p-\varepsilon_0^p) \tag{41}$$

When applying the least-square error fitting method, the value of *A* in Eq.(41) can be obtained as

$$A = \frac{n\sum(xy) - \left(\sum x\right)\left(\sum y\right)}{n\sum(x^2) - \left(\sum x\right)^2} \tag{42}$$

where n is a number of experimental data points.

Finally from Eq.(38) and Eq.(42), we can obtain the material parameters C and γ.

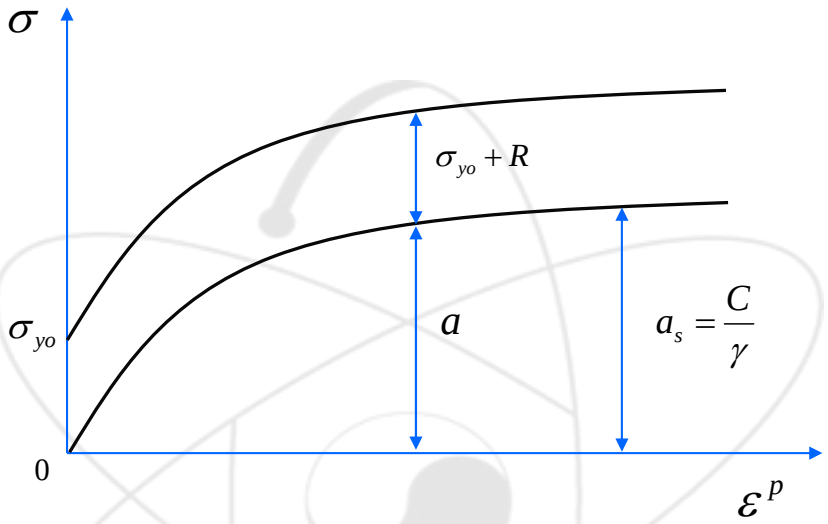

Fig. 8 Half Cycle of Stress-Strain Data for Material Parameter Identification

2.2.3 Chaboche 3-Decomposed Model

2.2.3.1 Constitutive Equations

To improve the deficiency of the Armstrong and Frederick model for a ratcheting simulation, Chaboche and his co-workers proposed a 'decomposed' nonlinear kinematic hardening rule as follows;

$$\dot{\alpha}_{ij} = \sum_{k=1}^{n}(\dot{\alpha}_{ij})_k = \sum_{k=1}^{n}\left(\frac{2}{3}C_k\dot{\varepsilon}_{ij}^{p} - \gamma_k(\alpha_{ij})_k\dot{p}\right) \tag{43}$$

As expressed in Eq.(43), the Chaboche kinematic hardening model is basically a superposition of several Armstrong and Frederick hardening rules.

The plastic modulus coupled with this kinematic hardening model, which can be obtained through the same procedures of Eq. (19) to Eq. (30), can be expressed as

$$H = E_{ijkl}\frac{\partial f}{\partial \sigma_{ij}}\frac{\partial f}{\partial \sigma_{kl}} + \frac{2}{3}\sum_{k=1}^{n}(C_k)\frac{\partial f}{\partial \sigma_{ij}}\frac{\partial f}{\partial \sigma_{ij}} - \sum_{k=1}^{n}\left[\gamma_k(\alpha_{ij})_k\right]\frac{\partial f}{\partial \sigma_{ij}}\sqrt{\frac{2}{3}\frac{\partial f}{\partial \sigma_{ij}}\frac{\partial f}{\partial \sigma_{ij}}} + b(Q-R)\sqrt{\frac{2}{3}\frac{\partial f}{\partial \sigma_{mn}}\frac{\partial f}{\partial \sigma_{mn}}} \quad (44)$$

Initially, Chaboche proposed a model with 3-decomposed rules (n = 3), which has three segments of a stable hysteresis loop. This model suggests that the first rule (α_1) should have a very large modulus at beginning of the hardening behavior and stabilizes very quickly. The second rule (α_2) should have a function of simulating the transient nonlinear part. Finally, the third rule (α_3) should have a function of the linear hardening behavior of the hysteresis loop throughout all the strain ranges.

2.2.3.2 Cyclic Behavior

To investigate the cyclic behavior of the Chaboche model with 3-decomposed rules, the following material parameters are used [Bari, 2000]

Kinematic Hardening : $C_{1\text{-}3}$ = 60000, 12856, 455 (ksi)
$\gamma_{1\text{-}3}$ = 20000, 800, 9
Isotropic Hardening : $Q_M = Q_o$ = 0.0 ksi, b=0.0, μ=0.0
Yield Stress : σ_{yo} = 18.8 ksi
Young's Modulus : E = 26300 ksi
Poisson's Ratio : ν = 0.302

To provide ratchet loading conditions, the stress cycle with a mean stress is used as shown in Fig. 9. Fig. 10 shows the simulated stress-strain hysteresis loop. As shown in the figure, in some of the initial load cycles, the inelastic strains are relatively large but by increasing the number of cycles in a certain lever, the cyclic strain increments become stable and it reaches a steady rate of a ratcheting stain.

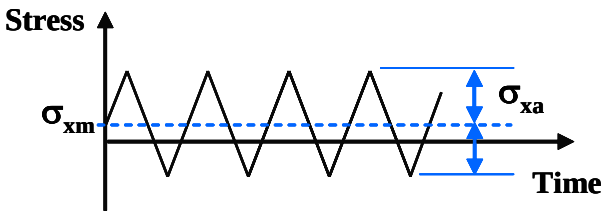

σ_{xa} = 32.0 ksi

σ_{xm} = 6.52 ksi

Fig. 9 Cyclic Loading History with Mean Stress

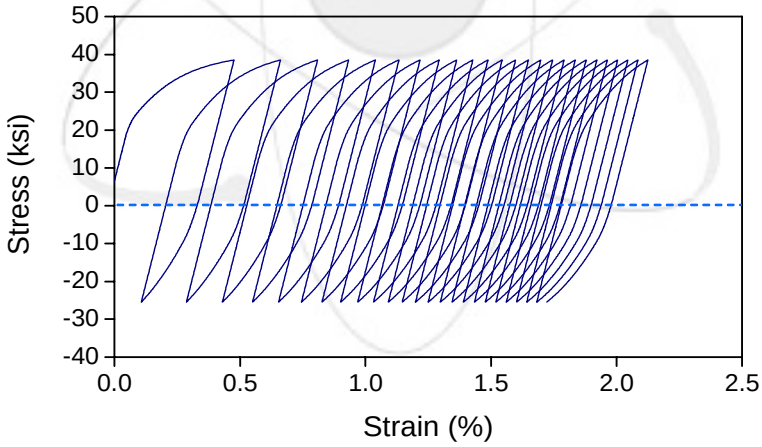

Fig. 10 Simulation Result of Cyclic behavior by the Chaboche 3-Decomposed Rule

Fig. 11 shows the traces of the 3-decomposed rules a_1, a_2, and a_3 (the total backstresses) and their sum resulting yield surface center a_x.

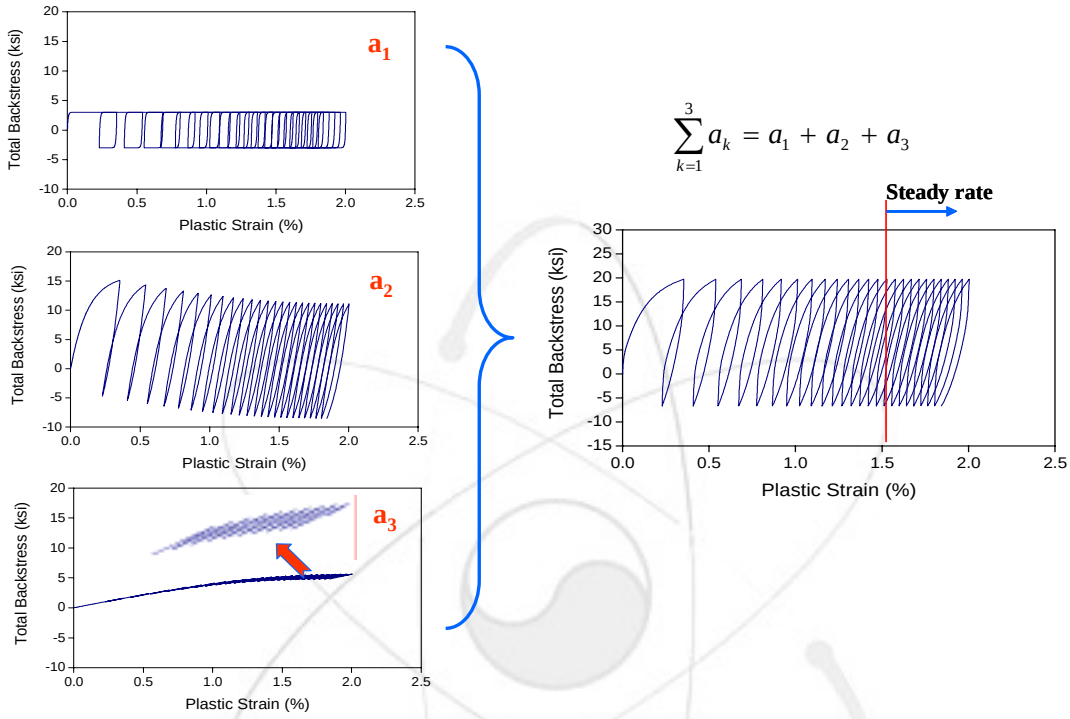

Fig. 11 Components of Total Backstress by the Chaboche 3-D Model

In this figure, we can see that each rule represents well its own function as described in the above section. Especially, it is observed that the constant ratcheting rate is mainly caused by an incorporation of the linear kinematic hardening rule of a_3 along with other nonlinear ones.

In third rule of a_3, when the value of γ_3 is zero, the complete shakedown of ratcheting occurs as shown in the results of Fig. 12.

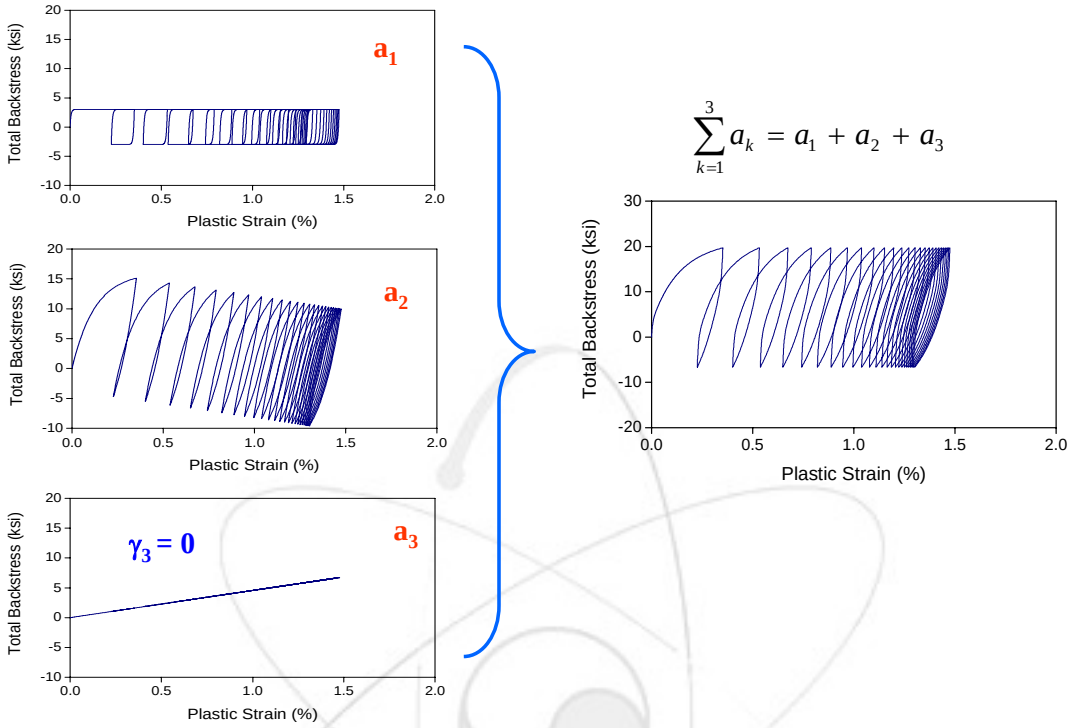

Fig. 12 Components of Total Backstress in Case of $\gamma_3 = 0$

This shakedown phenomena can be easily explained when we investigate any two points in the traces of the backstress components. Actually, when we neglect the value of γ_3, it is expected that the ratcheting strain will be overestimated for some initial cycles but underestimated gradually with the increasing number of cycles. To overcome this phenomenon, a slight nonlinearity can be introduced in the third rule by assigning a relatively small value of γ_3 as shown in Fig. 11. However, when increasing the value of γ_3, the third backstress reaches its limiting value quickly and the constant ratcheting rate begins much earlier. Furthermore, the larger the estimation of the value of γ_3, the higher the total accumulated ratcheting strain results in the simulation as shown in Fig. 13. With

considering all these characteristics, the parameter of γ_3 may be considered as a ratcheting parameter whose value can be determined with uniaxial ratcheting rate data.

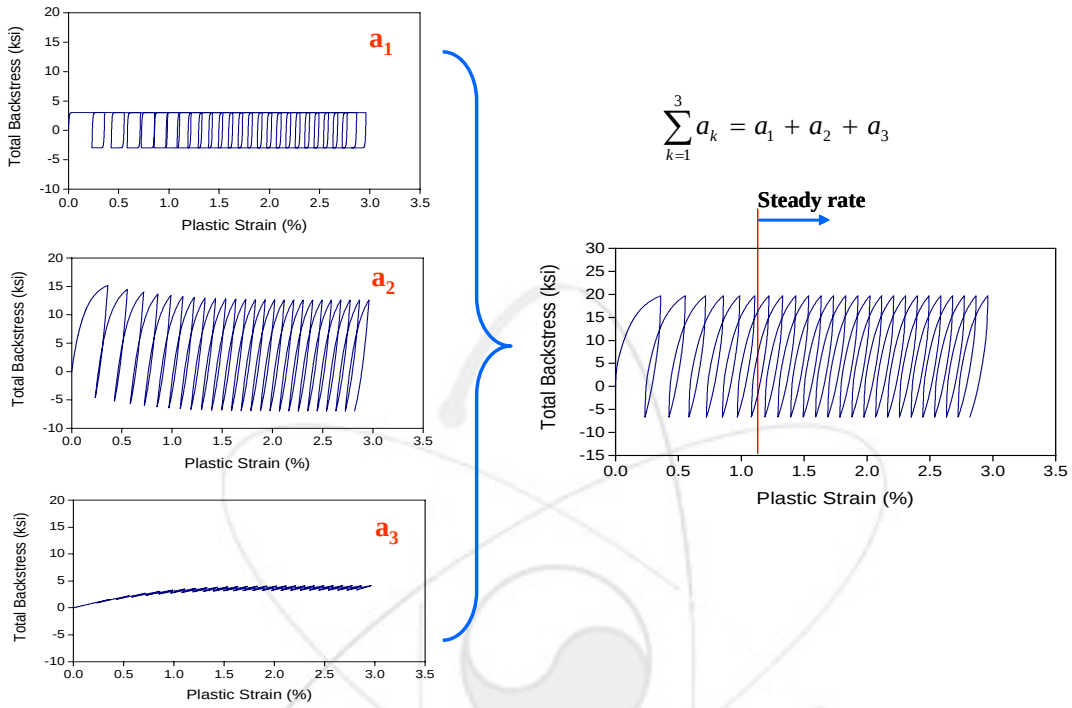

Fig. 13 Components of Total Backstress in Case of $\gamma_3 = 30$

Fig. 14 shows the mean stress effects on the uniaxial ratcheting behavior. As shown in the figure, the higher the value of the mean stress, the larger the ratcheting strain occurs. When there is no mean stress, a uniaxial ratcheting would not occur at all and the cyclic loadings result in a closed loop without translation of the yield surface. This loading condition, which can invoke the ratcheting behavior, may be occurred in the KALIMER-600 design as shown in Fig. 15. As shown in the figure, as a primary hot sodium free surface moves up (hot front condition), relatively small tension stress occurs in front of the moving hot free surface with a following large compression stress at location of the hot free surface. When the free surface moves down (cold front condition), the stress distributions throughout moving range are changed reversly. Therefore, as the free surface moves up and down periodically, the moving region will be subjected to stress cycles with a mean stress, which can invoke ratcheting.

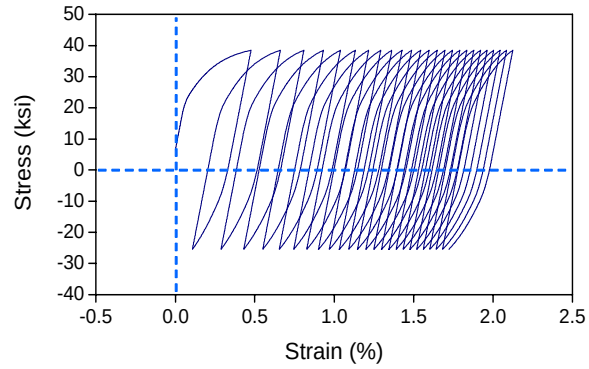

(a) σ_{xm} = 6.52 ksi

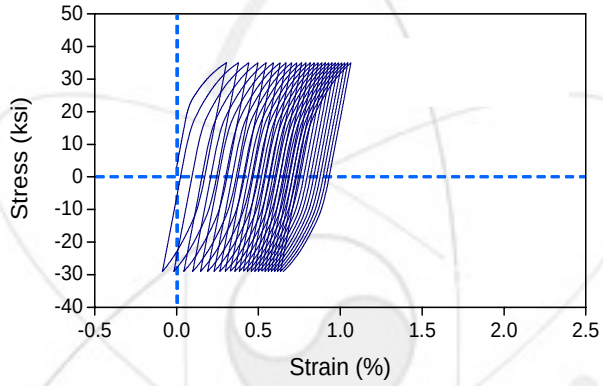

(b) σ_{xm} = 3.0 ksi

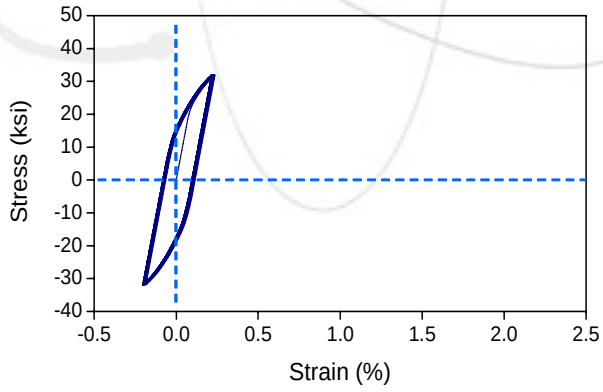

(c) σ_{xm} = 0.0 ksi

Fig. 14 Mean Stress Effects on Cyclic Behavior

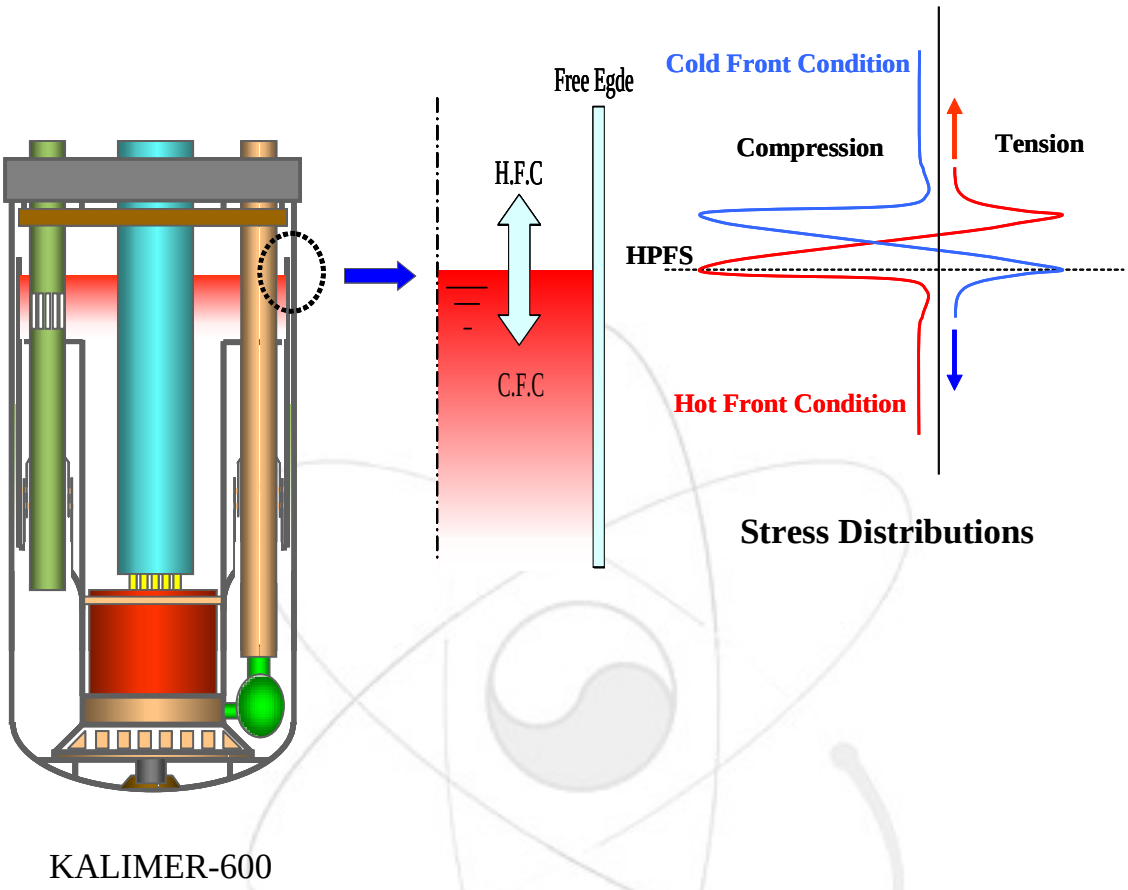

Fig. 15 Thermal Ratcheting Environments in KALIMER-600 Design

Fig. 16 shows the effect of the multiaxial loading conditions on the cyclic behavior. As shown in the figure, when each load of biaxial loads is exerted in-phase direction, the accumulated ratcheting strain becomes smaller than the uniaxial load (Fig. 16(b)). However, when each load of the biaxial loads is applied out-of-phase direction, the ratcheting strain significantly increases when compared with that of the uniaxial load (Fig. 16(c)).

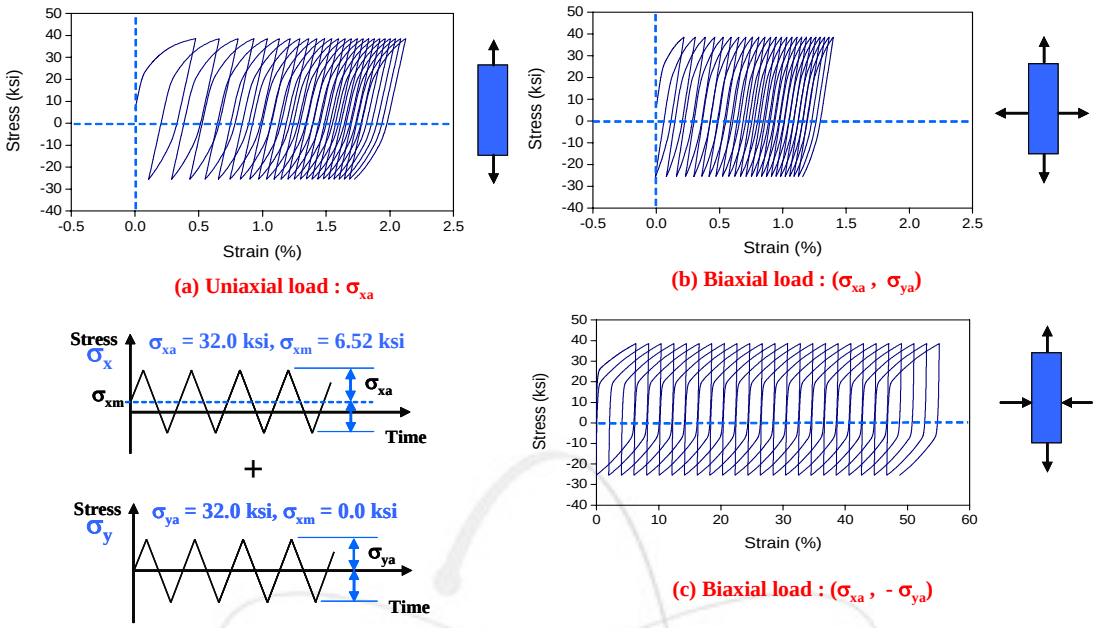

Fig. 16 Multi-axial Loading Effects on Cyclic Behavior

2.2.3.3 Parameter Identification

All parameters except for γ_3 related with the constitutive equation can be extracted from an experimental data of a uniaxial strain-controlled stable hysteresis loop. To use this data, the experiment should be performed with a reasonable strain limit to obtain the stabilized hysteresis loop.

The stabilized hysteresis loop for the loading part of the hardening curves should satisfy the following equations as

$$\sum_{k}^{n} a_k + \sigma_{yo} = \sigma_x \tag{45}$$

$$a_k = \frac{C_k}{\gamma_k}\left[1 - 2e^{-\gamma_k(\varepsilon^p - (-\varepsilon_L^p))}\right], \quad \text{for } k = 1 \text{ and } 2 \tag{46}$$

where ε_L^p is a strain limit of the stable hysteresis loop. Actually, to find the stable hysteresis loop and its strain limit, one can perform the stain-controlled uniaxial cyclic

experiments with increasing the strain amplitude cycle by cycle as shown in Fig. 17. From the figure, it would be determined the strain limit as about 0.85% which results in the stable hysteresis loop.

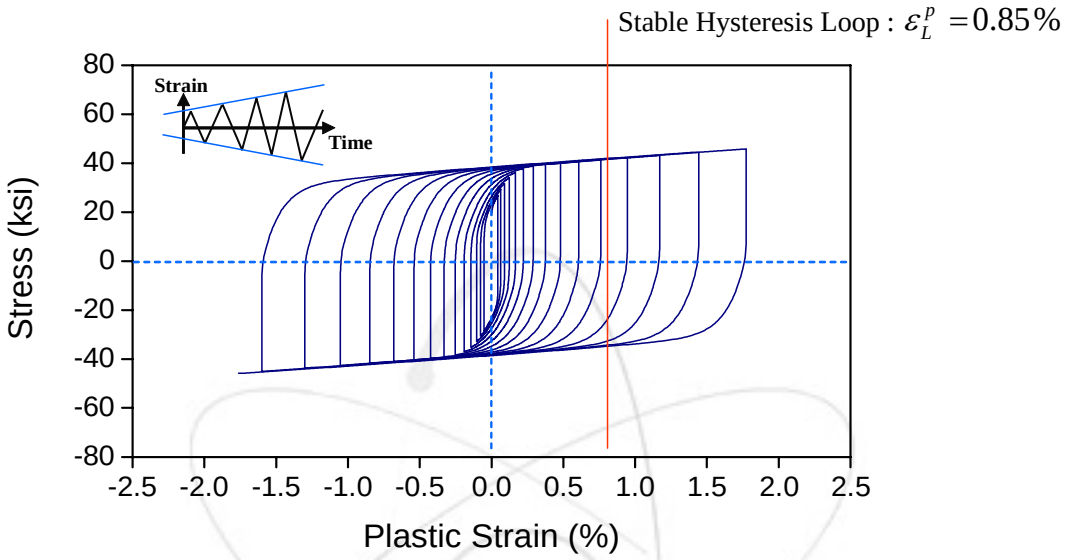

Fig. 17 Strain-Controlled Uniaxial Cyclic Behavior
with Increasing Input Amplitude

From an experimental data of the stable hysteresis loop of Fig. 18, a role of the backstress a_1 is to describe an initial stiff behavior after the yielding. Therefore, the parameter C_1 should be a large value to describe the plastic modulus at the yielding region and corresponding parameter γ_1 also should be large enough to stabilize the hardening of the backstress a_1 immediately. These parameters can be determined with the engineering sense by the user. The role of the backstress a_3 is to describe the linear part at a high strain region as shown in Fig. 18. Therefore, the parameter C_3 should describe the plastic modulus at a high strain range, and can be determined from the slope of the linear segment of a hysteresis loop. With the determined parameters C_1, γ_1, and C_3, the parameters C_2 and γ_2 can be determined by trial simulations to produce a good representation of the experimental stable hysteresis loop which satisfy the following relationship

$$\frac{C_1}{\gamma_1}+\frac{C_2}{\gamma_2}+\sigma_{yo}=\sigma_x-\frac{C_3}{2}\left\{\varepsilon_x^p-(-\varepsilon_L^p)\right\} \tag{47}$$

at or close to the strain limit ε_L^p. In these trial simulations, it can be done without the parameter γ_3 because this parameter has a significant effect on the ratcheting rate but not on the stable hysteresis loop.

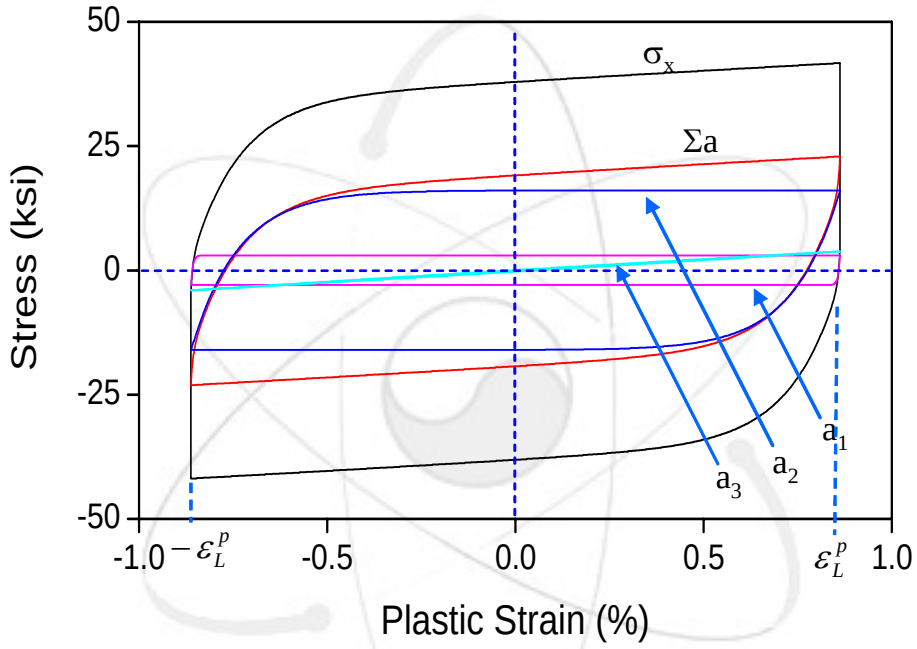

Fig. 18 Stable Hysteresis Loop to Obtain the Material Parameters

Fig. 19 shows the results of trial simulations with variations of γ_2 with C_1=60000 ksi, γ_1=20000, C_3= 455 ksi, γ_3=0.

To obtain the parameter γ_3, it is necessary to perform a uniaxial ratcheting experiment. Using this data (ε^p vs N), γ_3 can be determined by trial simulations to produce a good stable ratcheting rate.

Fig. 20 shows the result of a verification simulation with finally determined parameters. As shown in the figure, the Chaboche 3-decomposed model provides a good

agreement with that of the experiment but it still underestimates the plastic modulus at the yielding region.

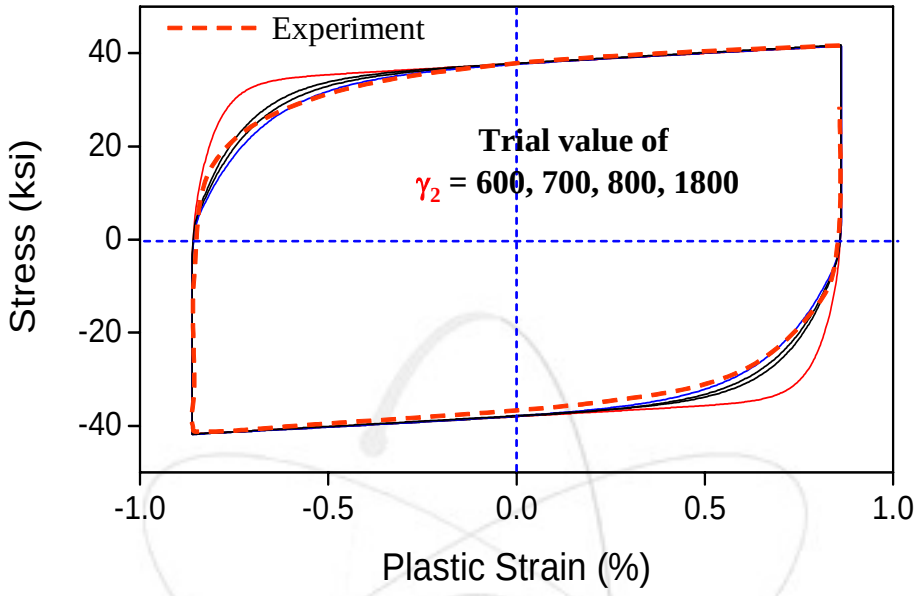

Fig. 19 Trial Simulations to Obtain the Best γ_3 Value

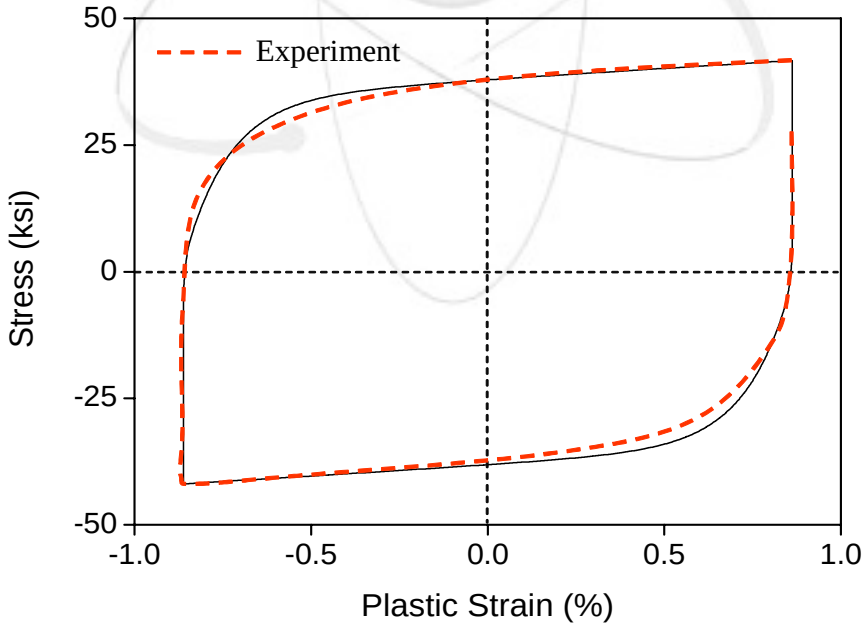

Fig. 20 Verification Simulation with Final Material Parameters

2.2.4 Chaboche Model with A Threshold

2.2.4.1 Constitutive Equations

To overcome the deficiencies of the Chaboche 3-decomposd model, Chaboche proposed a 4-decomposed nonlinear hardening rule with a concept of a 'threshold' as follows (Chaboche, 1991);

$$\dot{\alpha}_{ij} = \sum_{k=1}^{4} (\dot{\alpha}_{ij})_k = \sum_{k=1}^{4} \left(\frac{2}{3} C_k \dot{\varepsilon}_{ij}^{p} - \gamma_k (\alpha_{ij})_k \left\langle 1 - \frac{\mathrm{A}_k}{f(a_k)} \right\rangle \dot{p} \right) \tag{48}$$

In the above equation, the constants A_1, A_2, and A_3 are zero and only A_4 has a constant value. The $f(a_k)$ means the yield function represented as $f(a_k)=[(3/2)(a_k \bullet a_k)]^{1/2}$. This rule gives a linearly growing kinematic hardening behavior to a certain threshold stress level and it becomes a nonlinear behavior outside the threshold level. Therefore, it is possible to enhance the plastic modulus within a certain range after the yielding.

The extracted plastic modulus coupled with this kinematic hardening model can be expressed as

$$H = E_{ijkl} \frac{\partial f}{\partial \sigma_{ij}} \frac{\partial f}{\partial \sigma_{kl}} + \frac{2}{3} \sum_{k=1}^{n} (C_k) \frac{\partial f}{\partial \sigma_{ij}} \frac{\partial f}{\partial \sigma_{ij}} - \sum_{k=1}^{n} \left[\gamma_k (\alpha_{ij})_k \left\langle 1 - \frac{A_k}{f(a_k)} \right\rangle \right] \frac{\partial f}{\partial \sigma_{ij}} \sqrt{\frac{2}{3} \frac{\partial f}{\partial \sigma_{ij}} \frac{\partial f}{\partial \sigma_{ij}}} + b(Q-R) \sqrt{\frac{2}{3} \frac{\partial f}{\partial \sigma_{mn}} \frac{\partial f}{\partial \sigma_{mn}}} \tag{49}$$

2.2.4.2 Cyclic Behavior

As an example of an application, the parameters used in this model are as follows (Bari, 2000];

Kinematic Hardening : $C_{1\text{-}4}$ = 60000, 3228, 455, 15000 (ksi)

$\gamma_{1\text{-}4}$ = 20000, 400, 11, 5000

A_4 = 5.0 ksi

Isotropic Hardening : $Q_M = Q_o$ = 0.0 ksi, b=0.0, μ=0.0

Yield Stress : σ_{yo} = 18.8 ksi

Young's Modulus : E = 26300 ksi

Poisson's Ratio : ν = 0.302

Fig. 21 shows the calculated total backstress components for a stress amplitude 32 ksi with a mean stress 6.52 ksi. As shown in the figure, the roles of the backstresses a_1, a_2, and a_3 are the same as those of the Chaboche 3-decomposed model and a backstress a_4 represents a stiff plastic modulus to a certain threshold stress level and it stabilizes its hardening behavior outside the threshold level.

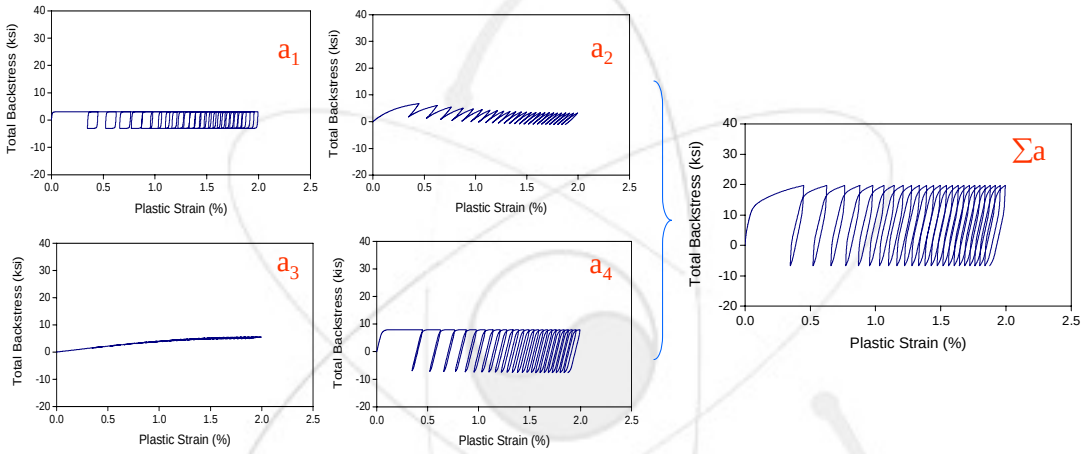

Fig. 21 Components of Total Backstress by the Chaboche 4-Decomposed Model

Fig. 22 shows the stress-controlled cyclic behavior of a stress-strain relationship. In this result, it is evident that this model can improve the hardening region with a combination of a linear and a nonlinear hardening model. When the linearly increasing hardening stress reaches the threshold level A_4, the hardening becomes nonlinear again and the reduction of ratcheting is attenuated to avoid potential shakedown. Therefore, the material parameter A_4 can be considered as a ratcheting parameter which should be determined from uniaxial ratcheting experimental data. Fig. 23 shows the comparison of the strain-controlled hysteresis loops between the Chaboche 3-decomposed model and the Chaboche 4-decomposed model.

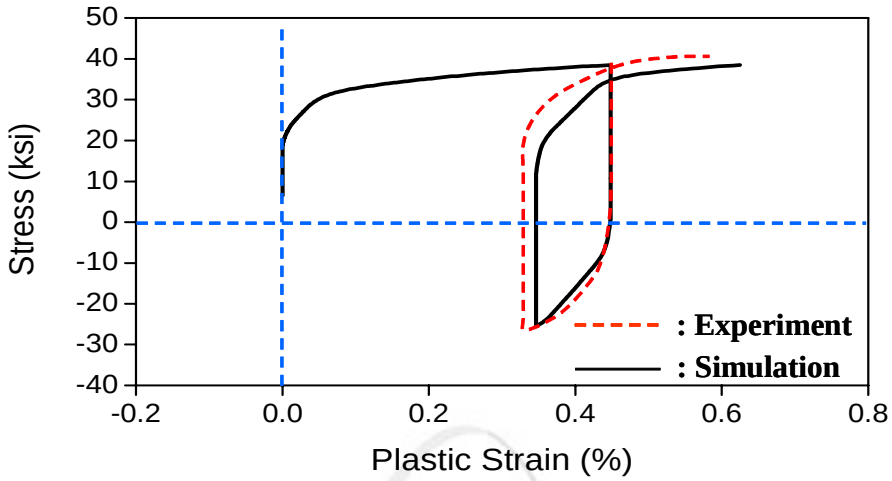

Fig. 22 Comparison of Stress-Controlled Hysteresis Loops

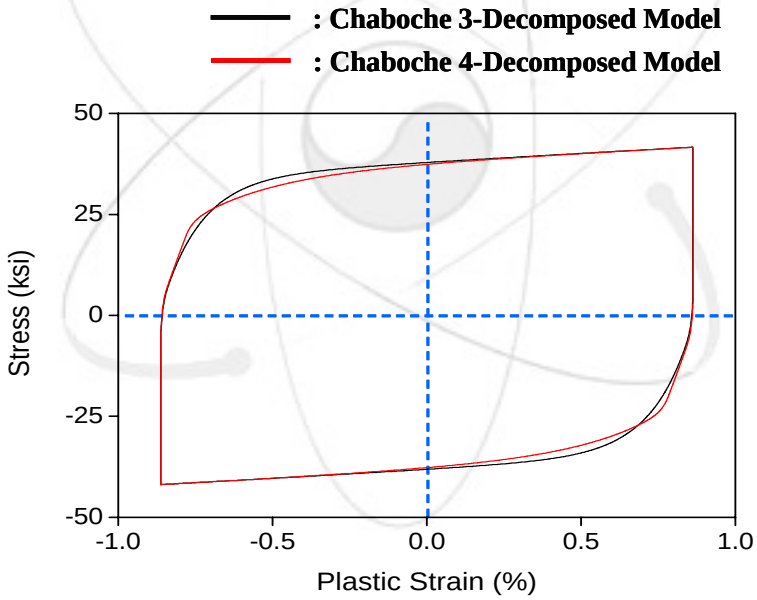

Fig. 23 Comparison of Strain-Controlled Hysteresis Loops

2.2.4.3 Parameter Identifications

Fig. 24 shows the strain-controlled total backstress components. As shown in the figure, the material parameters C_1, γ_1, C_3, and γ_3 can be determined by using the same method as described in the Chaboche 3-decomposed model. The parameters of C_2, γ_2, C_4,

and γ_4 are identified by trials to give a good result with the experimental stable hysteresis loops which satisfy the following relationship at or close to the strain limit ε_L^p

$$\frac{C_1}{\gamma_1}+\frac{C_2}{\gamma_2}+\frac{C_4}{\gamma_4}+A_4+\sigma_{yo}=\sigma_x-\frac{C_3}{2}\left\{\varepsilon_x^p-(-\varepsilon_L^p)\right\} \tag{50}$$

To start a trial simulation, the first trial value of A_4 can be taken close to the value of the mean stress in the uniaxial ratcheting experiment used for a parameter identification (Chaboche, 1991). After determining the parameters C_2, γ_2, C_4, and γ_4, which produce a good agreement with the strain-controlled experimental stable hysteresis loop, with the first trial value of A_4, further simulations are to be performed with variation of A_4 values to improve the simulation result matching the ratcheting experimental data. In this simulation finding a final value of A_4, the strain-controlled stable hysteresis loop should not be deteriorated due to the selected value of A_4.

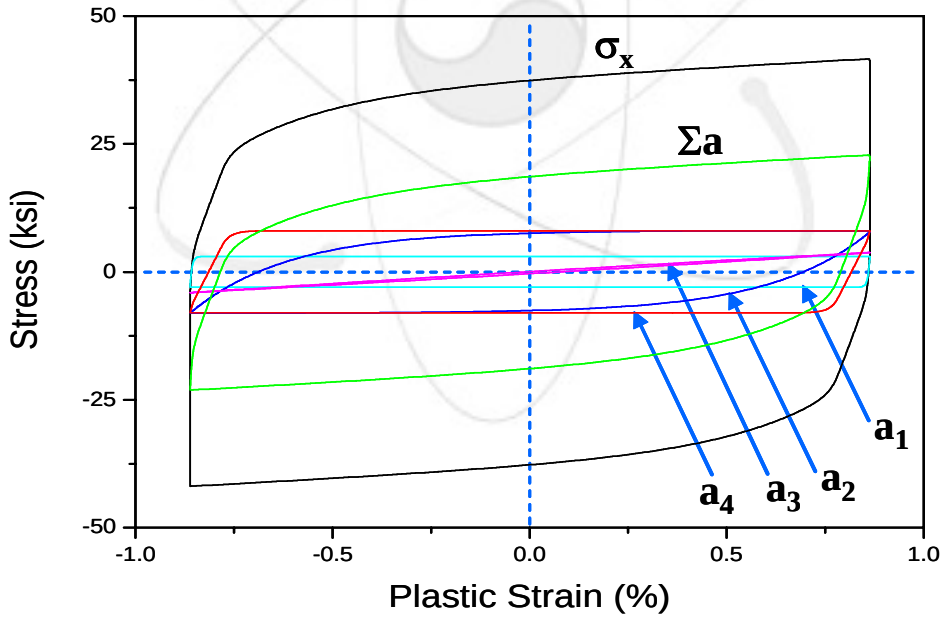

Fig. 24 Stable Hysteresis Loop by the Chaboche 4-Decomposed Model

2.2.5 Ohno and Wang Model

2.2.5.1 Constitutive Equations

Ohno and Wang proposed the multi-decomposed nonlinear kinematic hardening rules based on dividing the hardening curve into many linear segments like the multilinear hardening model. They introduce a slight nonlinearity for each decomposed rule at the transition from a linear kinematic hardening to the stabilized critical state as follows;

$$\dot{\alpha}_{ij} = \sum_{k=1}^{n} (\dot{\alpha}_{ij})_k = \sum_{k=1}^{n} \left\{ \frac{2}{3} C_k \dot{\varepsilon}_{ij}^{p} - \gamma_k (\alpha_{ij})_k \left\langle \dot{\varepsilon}_{ij}^{p} \bullet \frac{(\alpha_{ij})_k}{f(a_k)} \right\rangle \left(\frac{f(a_k)}{C_i / \gamma_i} \right)^{m_i} \right\} \tag{51}$$

In the above equation, the slight nonlinearity is expressed with the multiplier with a power of m_i and it has a role of preventing the stress-controlled hysteresis loop from being closed loop and causing a ratcheting behavior.

Coupled with the above kinematic hardening rule through a consistency condition, the plastic modulus can be expressed as follows;

$$H = E_{ijkl} \frac{\partial f}{\partial \sigma_{ij}} \frac{\partial f}{\partial \sigma_{kl}} + \frac{2}{3} \sum_{k=1}^{n} (C_k) \frac{\partial f}{\partial \sigma_{ij}} \frac{\partial f}{\partial \sigma_{ij}} - \sum_{k=1}^{n} \left[\gamma_k (\alpha_{ij})_k \left\langle \frac{\partial f}{\partial \sigma_{ij}} \bullet \frac{(\alpha_{ij})_k}{f(a_k)} \right\rangle \left(\frac{f(a_k)}{C_k / \gamma_k} \right)^{m_i} \right] \frac{\partial f}{\partial \sigma_{ij}} + b(Q - R) \sqrt{\frac{2}{3} \frac{\partial f}{\partial \sigma_{mn}} \frac{\partial f}{\partial \sigma_{mn}}} \tag{52}$$

2.2.5.2 Cyclic Behavior

Ohno and Wang model requires a large number of the decomposed rules to make a good representation of the stabilized hysteresis curve. In this study, the example of simulation is carried out using 12-decomposed rules with following material parameters (Bari, 2000).

$C_{1\text{-}12}$ = 31940, 36214, 2520, 376, 11021, 4551, 3475, 2196, 857, 247, 98, 200 (ksi)

$\gamma_{1\text{-}12}$ = 45203, 13944, 7728, 4955, 3692, 2135, 1230, 585, 295, 119, 50, 20

m_i = 0.45

Isotropic Hardening : $Q_M = Q_o$ = 0.0 ksi, b=0.0, μ = 0.0

Yield Stress : σ_{yo} = 18.8 ksi

Young's Modulus : E = 26300 ksi

Poisson's Ratio : ν = 0.302

Fig. 25 and Fig. 26 show the simulation results of the stress-controlled and the strain-controlled cyclic behavior respectively. These simulation results will be compared and discussed with those of the other models on next section.

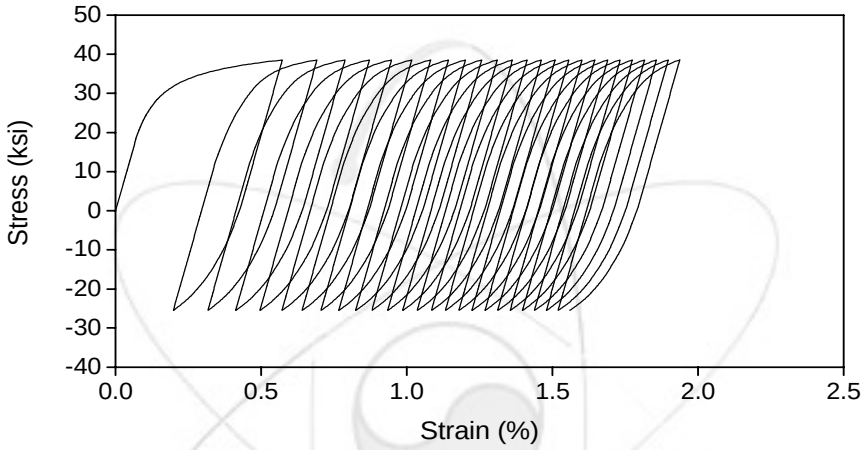

Fig. 25 Stress-Controlled Cyclic Behavior by the Ohno and Wang Model

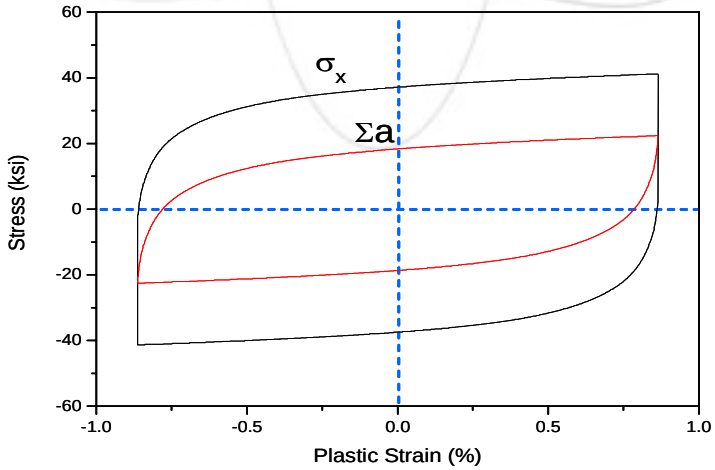

Fig. 26 Strain-Controlled Hysteresis Loop by the Ohno and Wang Model

Fig. 27 shows the strain-controlled cyclic behavior including the isotropic hardening parameters of $Q_M = Q_o = 37.7$ ksi, b=100.8, μ =0.5. Fig. 28 shows the effect of the parameter m_i on the rate of ratcheting. As show in the figure, it is evident that the smaller the value of m_i, the higher the rate of ratcheting. This means that by decreasing the value of m_i, the effect of nonlinearity induced by it becomes larger.

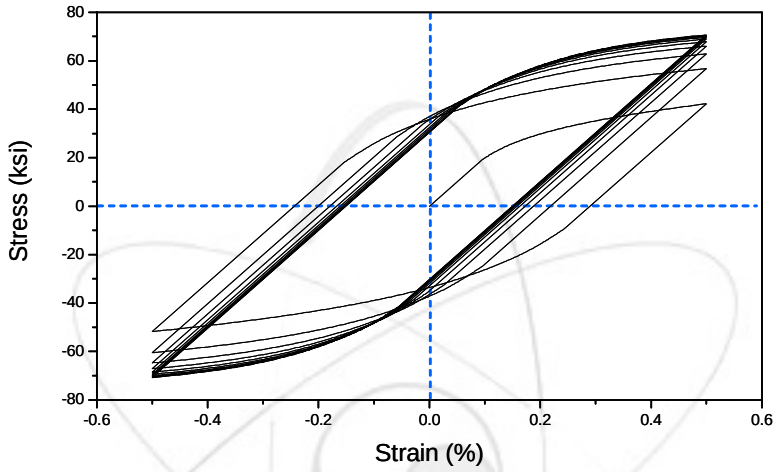

Fig. 27 Strain-Controlled Cyclic Behavior with Isotropic Hardening

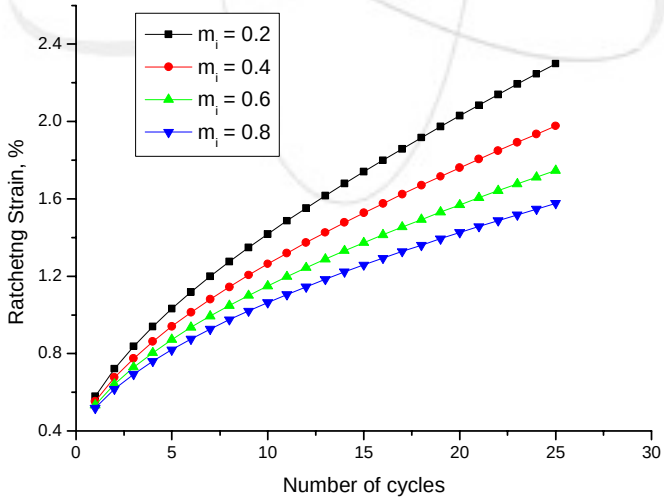

Fig. 28 Effect of Parameter m_i on the Rate of Ratcheting

2.2.5.3 Parameter Identifications

The required experimental data for the parameter identifications are a uniaxial stabilized hysteresis loop and a uniaxial ratcheting data. To identify the parameters from the stable hysteresis loop, the loading curve part should be divided into several segments as shown in Fig. 29 and the parameters of C_k and γ_k for each segment can be obtained by the following equations;

$$C_k = \frac{\sigma_x^k - \sigma_x^{k-1}}{\varepsilon_k^p - \varepsilon_{k-1}^p} - \frac{\sigma_x^{k+1} - \sigma_x^k}{\varepsilon_{k+1}^p - \varepsilon_k^p} \quad for\ k \neq 1, \tag{53}$$

$$\gamma_k = \frac{2}{\varepsilon_k^p + \varepsilon_0^p} \tag{54}$$

Finally, C_1 can be identified by the relationship as

$$\sum_{k=1}^{n} \frac{C_k}{\gamma_k} + \sigma_{yo} = \sigma_x^0 \tag{55}$$

and the values of the power m_i are assumed to be same for all segments and should be identified by a uniaxial ratcheting experimental data.

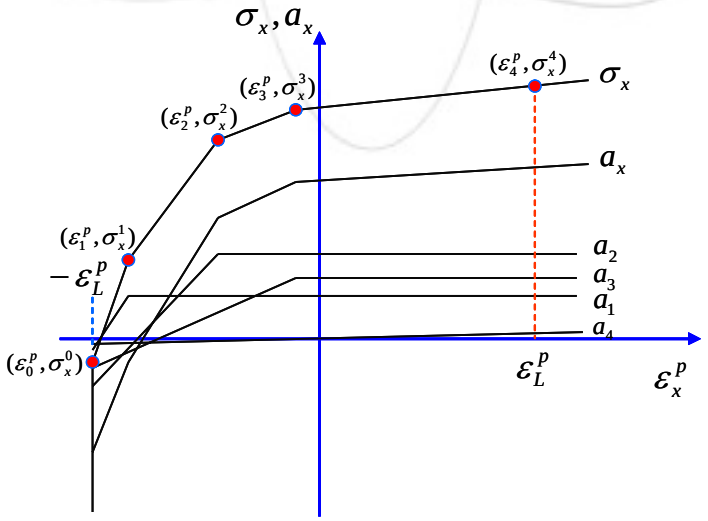

Fig. 29 Decomposed Hardening Concepts for the Ohno and Wang Model

In the Ohno and Wang model, the last hardening rule (α_n) has a similar effect of the ratcheting parameters as described in the Chaboche model. If the used strain-controlled stable hysteresis loop has a small strain range, the last backstress early reaches its plateau at ε_L^p and the parameter γ_n calculated by Eq.(54) becomes relatively large. This may result in over-prediction of ratcheting in some cases. Therefore, a hysteresis curve with reasonably large strain range should be used to resolve this problem. If a small strain range data is only available, the asymptotical extension technique of the strain range up to ε_s^p can be introduced as shown in Fig. 30.

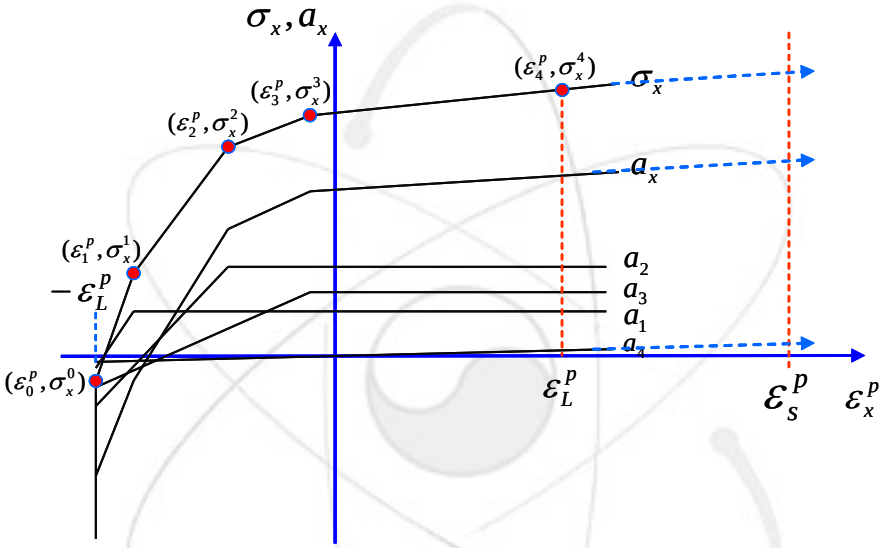

Fig. 30 Modified Concepts to Identify Material Parameters

2.3 Comparison Study

2.3.1 Stress-Controlled Behavior

The stress-controlled hysteresis loops calculated by the above constitutive models such as the Armstrong and Frederick model, the Chaboche 3-decomposed model, the Chaboche 4-decomposed model, and the Ohno and Wang model are compared with the experimental data published in a reference paper (Bari, 2000). As shown in Fig. 31(a), the hysteresis loop by a simple Armstron and Frederick model is very different from that of an experiment. On the other hand, the Chaboche 3-decomposed model shown in Fig. 31(b) predicts the cyclic behavior very well when compared to the experimental result

but it still shows a lower stiffness during the initial nonlinear part. The Chaboche 4-decomposed model overcomes the low stiffness problem occurring in the 3-decomposed Chaboche model as shown in Fig. 31(c). The hysteresis loop obtained by the Ohno and Wang model (Fig. 31(d)) shows a very good agreement with that of the experiment. This means that 12 segments used in this study are sufficient to simulate the hysteresis behavior accurately.

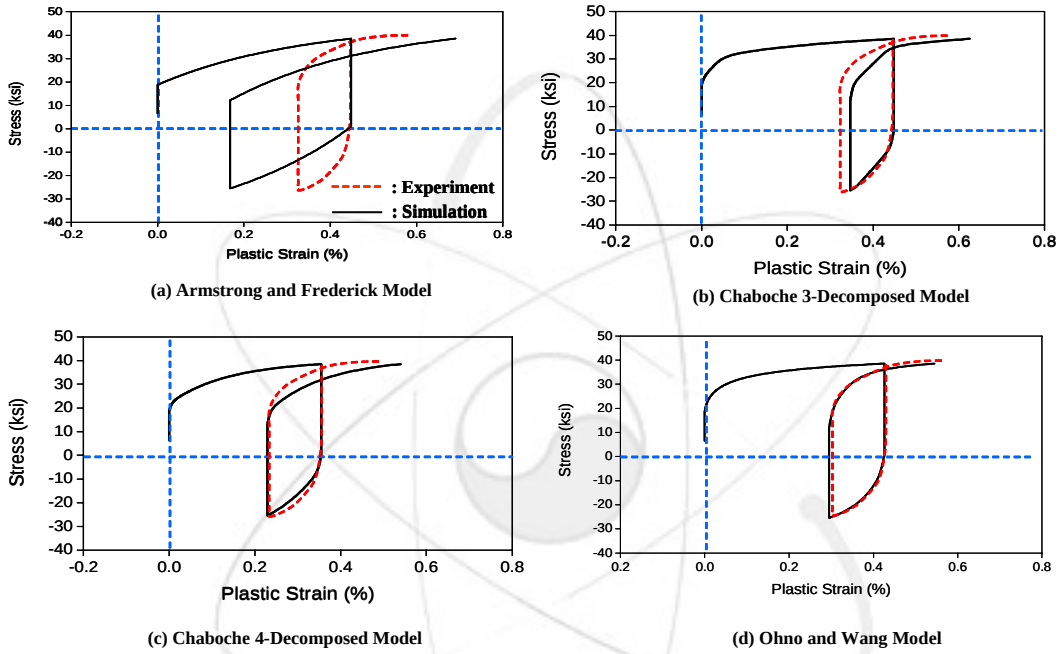

Fig. 31 Comparison of Stress-Controlled Cyclic Behavior

2.3.2 Strain-Controlled Behavior

Fig. 32 shows a comparison of the strain-controlled hysteresis loops obtained by each model. As shown in the figure, the Armstrong and Frederick model can not predict the nonlinear part accurately. The Chaboche models can describe the nonlinear behavior well but it still shows some discrepancies when compared to an experimental result in the nonlinear part. However, the hysteresis loop by the Ohno and Wang model shows a very good agreement with that of the experiment in the overall loop locus.

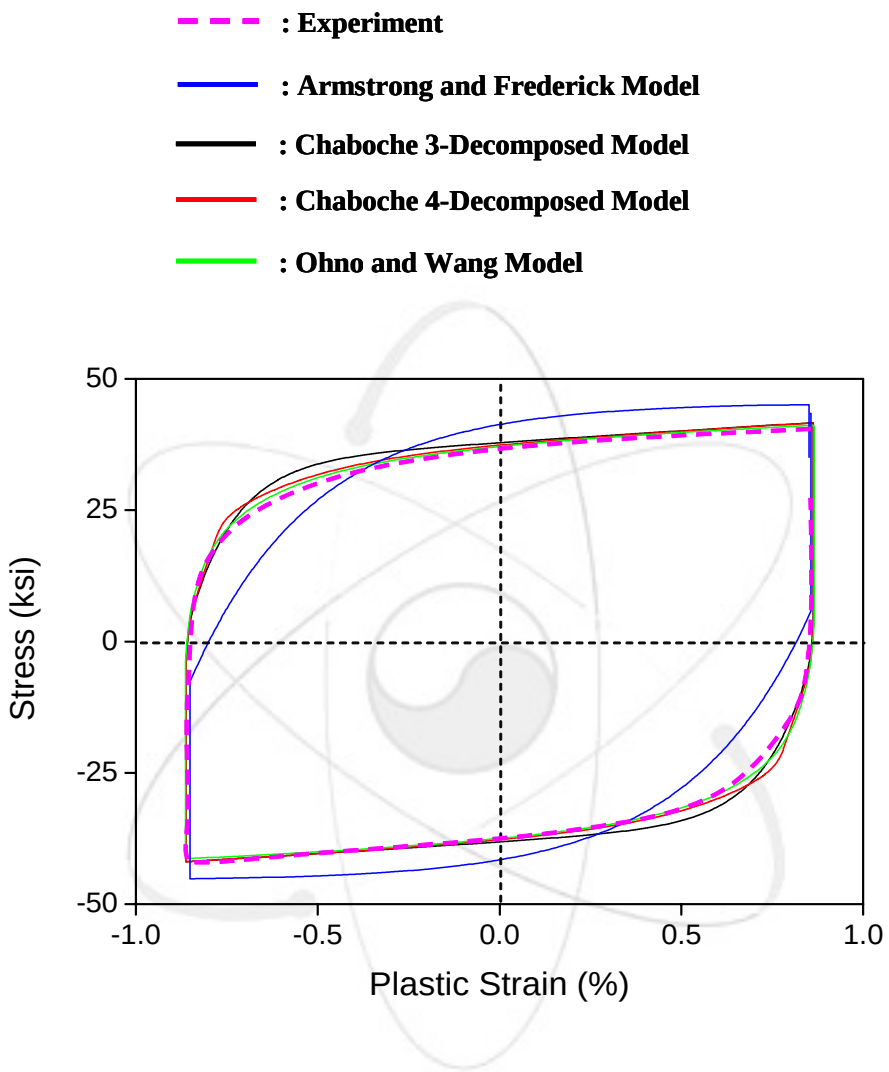

Fig. 32 Comparison of Strain-Controlled Hysteresis Loops for Each Model

2.3.3 Ratcheting Behavior

To compare the ratcheting strains obtained by each constitutive model, the maximum peak strain in each cycle is plotted as a function of the number of cycles. Fig. 33 shows the comparison of the ratcheting increments for each model. As shown in the figure, the Armstrong and Frederick model shows a significant over-predicting of a ratcheting. The Chaboche 3-decmposed rule shows a slightly different ratcheting accumulation during the initial cycles when compared to that of the Chaboche 4-decomposed rule but almost the same total accumulated strain after a couple of cycles. The overall simulation by these models still deviates from the experiments with an over-prediction. Among the constitutive models investigated in this study, it is revealed that the Ohno and Wang model provides the best uniaxial ratcheting prediction. Although this model predicts better in uniaxial ratcheting compared to the Chaboche model, it is known that this model still has over-prediction problems in the biaxial ratcheting simulations and in high stress levels.

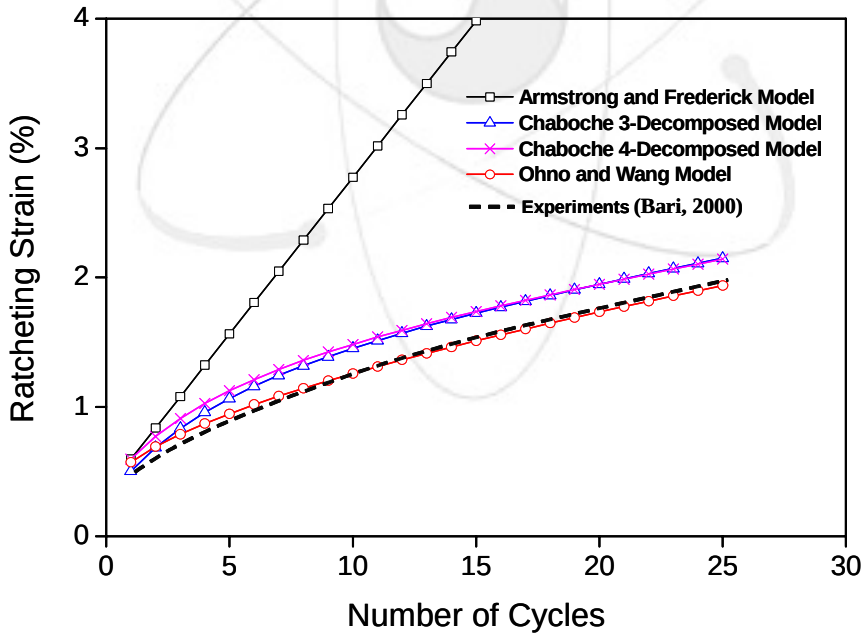

Fig. 33 Comparison of Ratcheting Simulations

3. Cyclic Viscoplasticity Constitutive Model

3.1 Unified Chaboche Model

In general, most materials have the time-dependent characteristics due to the viscous effects. We call this kind of a material behavior as viscoplasticity. For example of the stainless steels, it is well-known that the viscous effects, which invoke stress relaxation as well as strain rate dependency, can occur even in room temperature. Actually, the time-independent plasticity is a particular limiting case of viscoplasticity.

In unified theory which can simulate both of a cyclic loading and viscous behaviors, the total inelastic strain is described with the unified plastic and viscous strain term as follows;

$$\varepsilon^{in} = \varepsilon^{p} + \varepsilon^{v} = \varepsilon^{vp} \tag{56}$$

The unified Chaboche viscoplasticity model has a form combined with the nonlinear kinematic and isotropic hardening rules as follows;

$$\dot{\varepsilon}^{vp} = \left\langle \frac{|\sigma - \alpha| - R - \sigma_{yo}}{K} \right\rangle^{n} \operatorname{sgn}(\sigma - \alpha) \tag{57}$$

$$\dot{\alpha} = \sum_{k=1}^{m} \left(\frac{2}{3} C_k \dot{\varepsilon}^{vp} - \gamma_k \alpha_k \left| \dot{\varepsilon}^{vp} \right| \right) \tag{58}$$

$$\dot{R} = b(Q - R)\left| \dot{\varepsilon}^{vp} \right| \tag{59}$$

where x = [K, n, C_1, C_2, C_3, $C_{...}$, C_k, γ_1 γ_2, γ_3, $\gamma_{...}$, γ_k, b, Q, σ_{yo}] are material parameters and < > is the Macauley bracket. Total number of the material parameters identified for this model is actually dependent on the material types. The typically required experimental data to identify the material parameters contained in the unified viscoplastic constitutive equations are the Monotonic Tensile/Compression Tests, Cyclic Load Tests each with $\varepsilon(0) = 0$, and Stress Relaxation Tests [Furukawa, 2001].

The procedures performing the viscoplastic simulation can be briefly described in this study. First, with uniquely specified initial conditions such as

$$\varepsilon(0) = \varepsilon_0 \tag{60a}$$

$$\varepsilon^{in}(0) = \varepsilon_0^{in} \tag{60b}$$

$$\alpha(0) = \alpha_0 \tag{60c}$$

$$R(0) = R_0 \tag{60d}$$

The initial stress is calculated by the equation of

$$\sigma(0) = E(\varepsilon_0 - \varepsilon_0^{in}) \tag{61}$$

The subsequent states of the viscoplastic strain, backstress and drag stress can be obtained by the following equations after their rate of change are computed by Eqs. (57), (58), and (59).

$$\varepsilon^{vp}(k) = \varepsilon^{vp}(k-1) + \Delta t \cdot \dot{\varepsilon}^{vp}(k-1) \tag{62}$$

$$\alpha(k) = \alpha(k-1) + \Delta t \cdot \dot{\alpha}(k-1) \tag{63}$$

$$R(k) = R(k-1) + \Delta t \cdot \dot{R}(k-1) \tag{64}$$

For a strain-controlled simulation, the next state of stress σ(k) can be derived by the equation of

$$\sigma(k) = E[\varepsilon(k) - \varepsilon^{vp}(k)] \tag{65}$$

From the repetition of these processes, we can perform the entire computer simulation of the viscoplastic behavior of the material.

3.2 Examples of Application

The material in this study is 316L used in Chaboche 1989. The material parameters for the constitutive equations through Eq.(57) to (59) are as follows (Chaboche, 1989);

C_1 = 162400 MPa

C_2 = 6750 MPa

γ_1 = 2800

γ_2 = 25

Q = 60 MPa

b = 8

E = 185 GPa

σ_{yo} = 82 MPa

K = 151 MPa

n = 24

All initial conditions are assumed to be zero in this study. Among the viscous effects such as stress relaxation, creep strain increment, and strain rate dependency, first, the stress relaxation behavior is investigated with the strain-controlled simulations. Fig. 34 shows the strain-controlled hysteresis loop and Fig. 35 shows the stress-time history in case of the strain rate, 1.25×10^{-6} %/sec when there is no hold time. As shown in figures, we can see that the yield surface steadily increase during the initial cycles due to the isotropic hardening but there are no specific viscous behaviors something like the stress relaxation. Fig. 36 and Fig. 37 show the simulation results with same conditions but when there is a hold time during each cycle. In figures, we can see the evident viscous behavior of the stress relaxation at each cycle.

To see the behavior of the creep strain increment, the stress-controlled simulations are carried out. Fig. 38 shows the result of a stress-controlled hysteresis loop in case of no hold time. As shown in figure, the creep strain increment slightly occurs in ends of loading and unloading cycles. However, in case of with hold time, the significant creep strain increment occurs as shown in Fig. 39.

Finally, Fig. 40 shows the strain rate effects on monotonic tensile stress. As shown in figure, we can see that the strain rate significantly affects the material behavior and when the strain rate increases, more hardening behavior occurs in material.

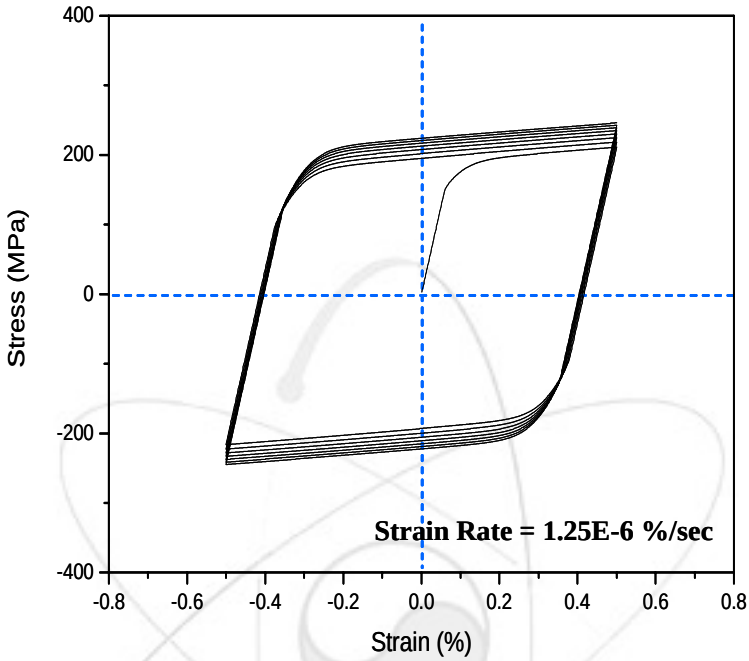

Fig. 34 Strain-Controlled Hysteresis Loop w/o Hold Time

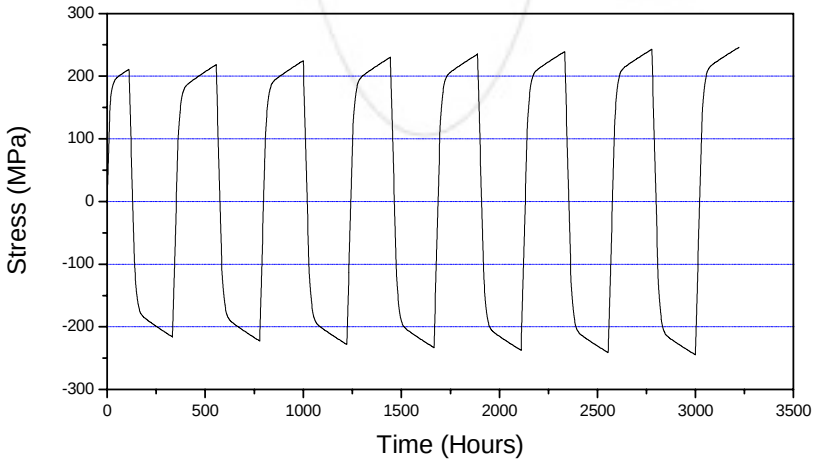

Fig. 35 Stress-Time History w/o Hold Time

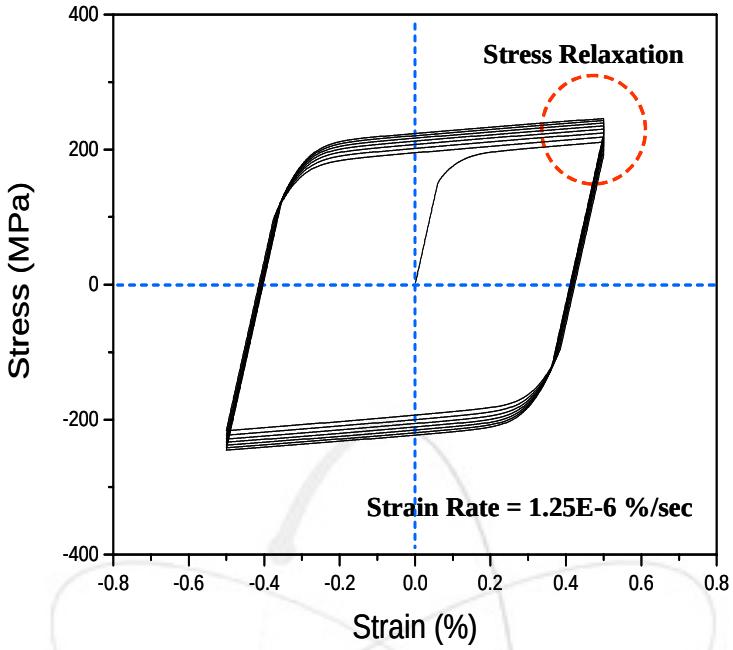

Fig. 36 Strain-Controlled Hysteresis Loop with Hold Time

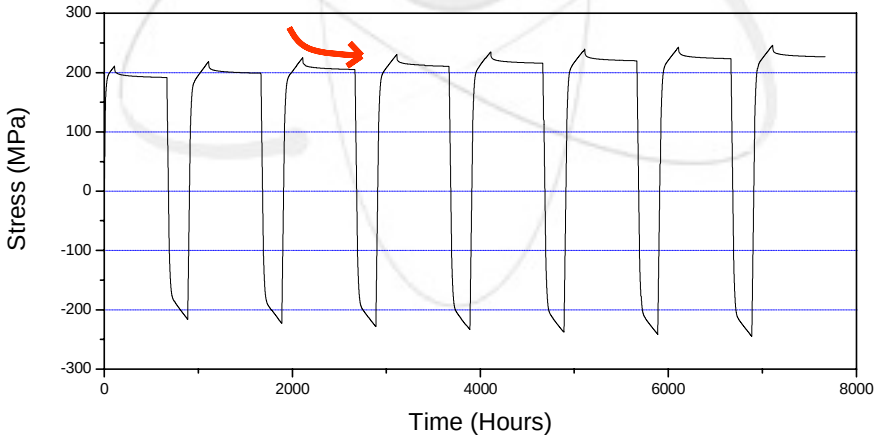

Fig. 37 Stress-Time History with Hold Time

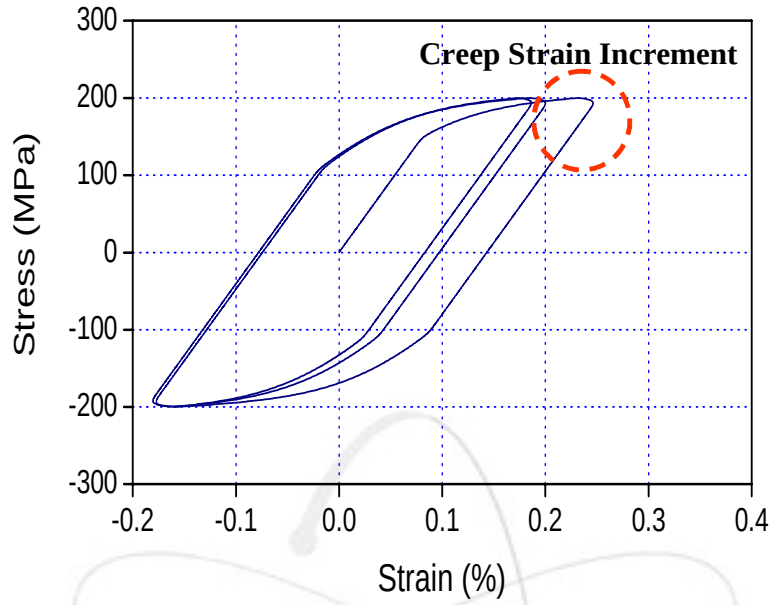

Fig. 38 Stress-Controlled Hysteresis Loop w/o Hold Time

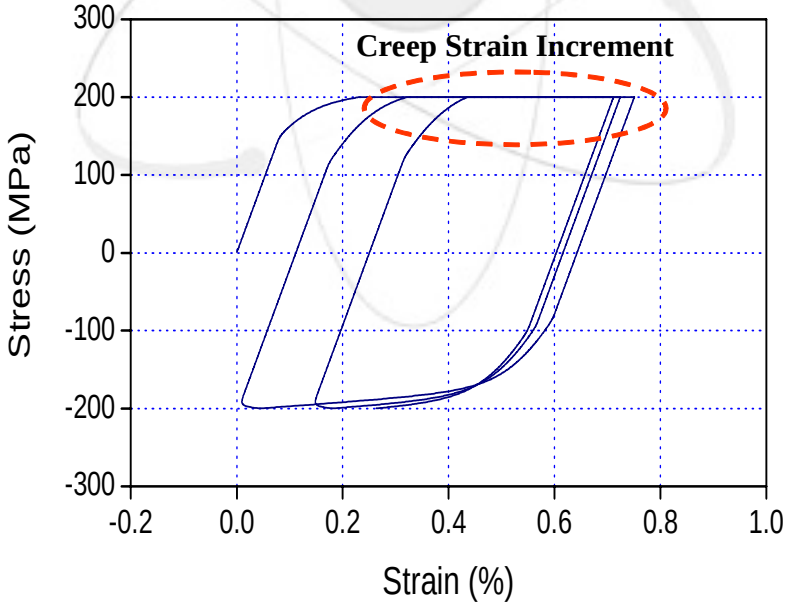

Fig. 39 Stress-Controlled Hysteresis Loop with Hold Time

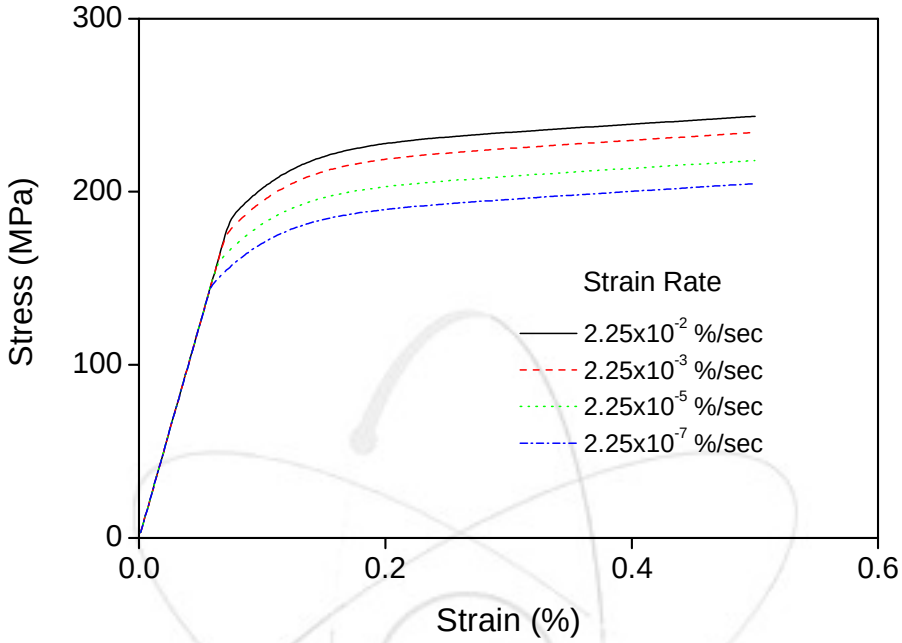

Fig. 40 Strain Rate Effect on Monotonic Hardening Behavior

4. PARA-ID Code

4.1 Salient Features of PARA-ID

The PARA-ID code is a general purpose computer simulation program for the nonlinear cyclic material behavior with and without viscous effects, which can simulate various constitutive models such as

- Prager Model
- Armstrong and Frederick Model
- Chaboche 3-decomposed rule Model
- Chaboche 4-decomposed rule Model
- Ohno and Wang Model
- Unified Chaboche Viscoplastic Model

The used language is Compaq Visual Fortran and the command based input data file system is applied.

4.2 General Procedures

Fig. 41 shows the general procedure of the PARA-ID code in case of the stress-controlled simulation. With PARA-ID code, we can simulate the nonlinear cyclic material behavior with both the stress-controlled and the strain-controlled options.

4.3 Input Commands and Formats

All commands supplied in PARA-ID are using the * commands. Under these command lines the input values are required to be written sequentially.

- ***TITLE** : user-defined evaluation title

  1. (TITLE)

  The title description can be written up to 80 characters.

- ***SLOAD** : input loading magnitude (3 x 3 matrix)

1. Lxx Lxy Lxz
2. Lyx Lyy Lyz
3. Lzx Lzy Lzz

- ***SMEAN** : input mean load (3 x 3 matrix)
  1. Lxx Lxy Lxz
  2. Lyx Lyy Lyz
  3. Lzx Lzy Lzz

- ***Young** : Young's modulus
  1. E

- ***POISS** : Poisson's ratio
  1. ν

- ***YIELD** : initial yield stress
  1. σ_{yo}

- ***AFKIN** : A-F model material parameters
  1. C, γ

- ***CB3KIN** : Chaboche 3-decomnposed model material parameters
  1. C_1, C_2, C_3
  2. γ_1, γ_2, γ_3

- ***CB4KIN** : Chaboche 4-decomnposed model material parameters
  1. C_1, C_2, C_3, C_4
  2. γ_1, γ_2, γ_3, γ_4
  3. A_4 (Threshold stress level)

- ***OWKIN** : Ohno and Wang model material parameters
  1. C_k (k=1,m)
  2. γ_k (k=1,m)
  3. m-value

- ***ISO** : isotropic hardening parameters
  1. b, Q_M, Q_0, μ

- ***VISCOPL** : unified Chaboche viscoplastic parameters
  1. K, n
  2. N (total number of solution step during hold time)
  3. T_1, T_2 (time interval for loading time, time interval for hold time)

- ***NLREV** : number of reverse loading cycles
  1. N

- ***NLDIV** : number of solution step during loading time
  1. N

- ***ITER** : the maximum number of internal iterations
  1. N

- ***CONVER** : hot and cold temperatures for the stress extremes
  1. convergence factor , maximum number of iteration

- ***OUTCTRL** : control data for the stored output data points on output files
  1. N

- ***SSREL** : stress-strain relationship
  1. N

- ***ETYPE** : element type (nodal degree of freedom)
  1. (OPTION)

  (OPTION = 1 : 6 degree)
  (OPTION ≠ 1 : 4 degree)

- ***LDINCF** : linear increasing factor of the reverse load
  1. factor

- ***SCALE** : scale factor for output stress unit
  1. factor

- ***END** : indicator of the end of input data (mandatory)

The typical format of input data file for the ratcheting simulation is as follows;

```
============================================================
AF STRAIN     ! Armstrong and Frederick model with strain-controlled
*TITLE
TEST          ! simulation title name
*SLOAD
1.5D-2 0. 0.      ! input strain magnitude, εxx=1.5%
0.       0. 0.
0.       0. 0.
*SMEAN
0.  0.   0.
0.  0.   0.
0.  0.   0.
*YOUNG
26300.D3
*POISS
```

```
0.302D0
*YIELD
18.8D3
*AFKIN
8000.D3 300.D0          ! C = 8000 ksi, γ = 300
*ISO
0.D0 37.7D6 37.7D6 0.D0
*NLREV
4                       ! total reverse loading = 4 (2 cycles)
*NLDIV
10000
*ITER
1000
*CONVER
1.D-3 1000
*OUTCTRL
20
*SSREL
3
*ETYPE
1.                      ! 6-dof system
*LDINCF
1.0D0                   ! no loading increment in reverse load cycles
*SCALE
1.D3                    ! output stress has ksi-unit
*END
============================================================
```

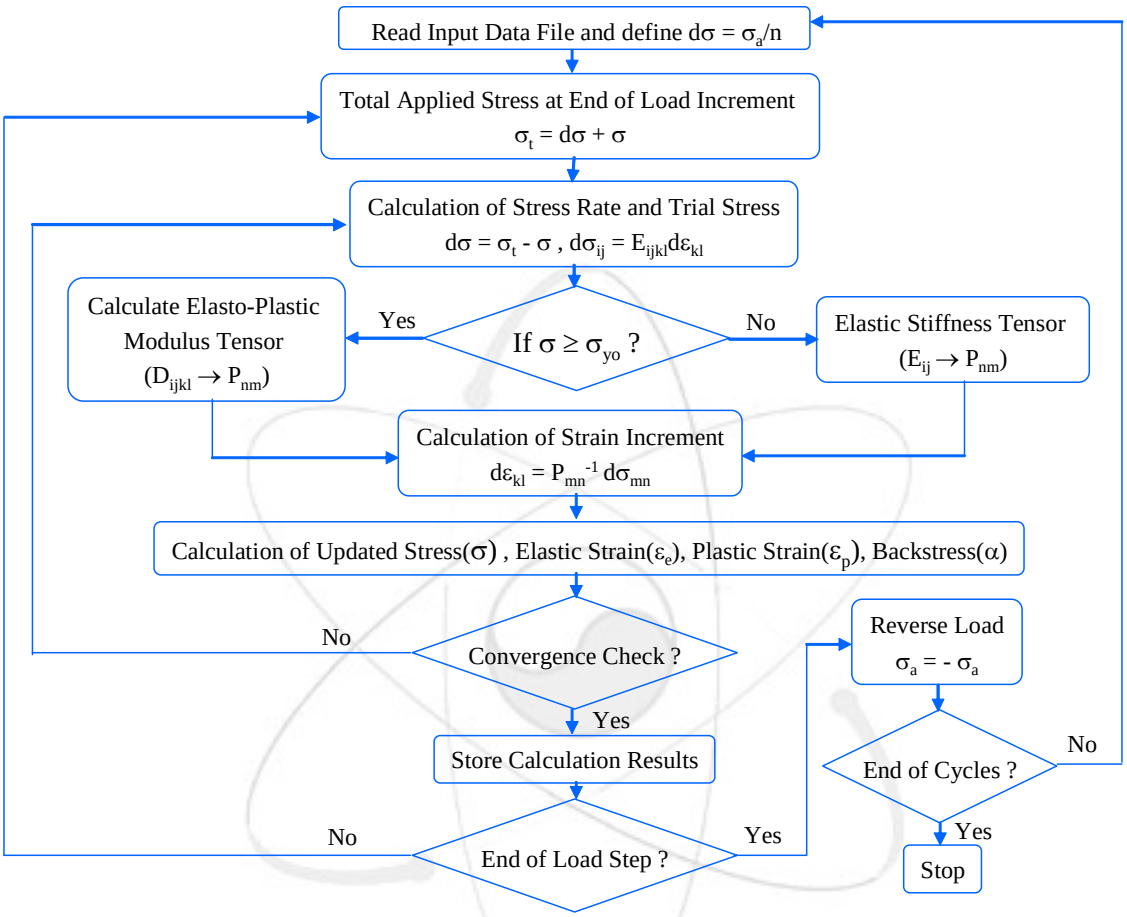

Fig. 41 General Procedures of PARA-ID Code (Stress-Controlled)

5. Conclusions

In development of the liquid metal reactors, which are operating in elevated temperature conditions, the structural integrity evaluations can be performed through the elastic analysis methods in compliance with the ASME-NH design rules. However, in some critical structural points, which can not satisfy the elastic analysis rules by the ASME-NH due to the conservatism contained in a design code, the inelastic analysis method is inevitably required to evaluate a total creep-ratcheting strain and the creep-fatigue damage limits. To apply this method to a real design, couples of uncertainties related with the nonlinear constitutive equations have to be resolved clearly. Among these works, the identification of the material parameters contained in the constitutive equations is very important to assure the accurate prediction of a nonlinear material behavior. In this study, the PARA-ID computer code, which has implemented various nonlinear constitutive models such as the Armstrong and Frederick model, the Chaboche 3-decomposed model, the Chaboche 4-decomposed model, the Ohno and Wang model, and the Unified Chaboche viscoplasticity model, is developed to be able to simulate multi-axial cyclic plasticity and viscoplasticity. Using this code, the cyclic ratcheting behavior and their material parameter identification methods are investigated with several examples of material. The developed PARA-ID code will be expected to be effectively used in the development of the nonlinear constitutive parameter identifications, especially for the high temperature liquid metal reactor development.

Acknowledgment

This project has been carried out under the Nuclear R & D Program by MOST.

Nomenclature

a_{ij} total backstress tensor

$\dot{a}_{ij}$ incremental total backstress tensor

a_k k component of total backstress

A_k threshold stress level

D_{ijkl} elasto-plastic modulus tensor

E Young's modulus

E_{ijkl} forth-order elastic modulus tensor

F loading function

dF loading increment

f yield function

$\dot{f}$ evolution of yield function

g plastic potential function

H generalized plastic modulus

m total number of decomposed kinematic hardening rules

m^i multiplier

$\dot{p}$ magnitude of plastic strain tensor (=$|\dot{\varepsilon}^p|$)

R drag stress

R_o initial drag stress

Δt time interval

α_{ij} deviatoric backstress tensor

$\dot{\alpha}_{ij}$ incremental deviatoric backstress tensor

α_o initial deviatoric backstress tensor

α_s stable backstress at $\dot{\alpha}=0$

ε_o initial strain tensor

ε strain tensor

ε_{ij} strain tensor

$\dot{\varepsilon}_{ij}^e$ elastic strain increment tensor

ε_o^{in} initial inelastic strain tensor

$\dot{\varepsilon}_{ij}^p$ plastic strain increment tensor

ε^{in} inelastic strain tensor

ε_L^p plastic axial strain amplitude of a strain-controlled hysteresis loop

ε^v viscous strain tensor

ε^{vp} viscoplastic strain tensor

$\dot{\varepsilon}^{vp}$ incremental viscoplastic strain tensor

σ stress tensor

σ_{ij} Cauchy stress tensor

$\dot{\sigma}_{ij}$ stress increment tensor

σ_{xa} amplitude of axial stress cycle

σ_{xm} mean of axial stress cycle

σ_{yo} initial yield stress

λ positive scale factor

τ_{ij} deviatoric stress tensor

ν Poisson's ratio

References

1995, ASME Boiler and Pressure Vessel Code Section III, Subsection NH, ASME.

1985, RCC-MR, Design and Construction Rules for Mechanical Components of FBR Nuclear Islands, AFCEN.

2003, Assessment Procedure for the High Temperature Response of Structures, British Energy Generation Ltd.

1984, Elevated Temperature Structural Design Guide for Class 1 Components of Prototype Fast Breeder Reactor, PNC N241-84-08, PNC.

1996, Creep-Fatigue Damage Rules for Advanced Fast Reactor Design, IAEA-TECDOC-933, IAEA.

Bari, S. and Hassan, T., 2000, "Anatomy of Coupled Constitutive Models for Ratcheting Simulation," Int. J. Plasticity, Vol. 16, pp. 381-409.

Bari, S. and Hassan, T., 2001, "Kinematic Hardening Rules in Uncoupled Modeling for Multiaxial Ratcheting Simulation," Int. J. Plasticity, Vol. 17, pp. 885-905.

Bari, S. and Hassan, T., 2002, "An Advancement in Cyclic Plasticity Modeling for Multiaxial Ratcheting Simulation," Int. J. Plasticity, Vol. 18, pp. 873-894.

Besseling, J.F., 1958, "A Theory of Elastic, Plastic and Creep Deformations of an Initially Isotropic Material," J. of Applied Mechanics, Vol. 25, pp.529-536.

Chaboche, J.L. and Rousselier, G., 1983, “On the Plastic and Viscoplastic Constitutive Equations – Part I: Rules Developed With Internal Variable Concept,” Journal of Pressure Vessel Technology, Vol. 105, pp.153-158.

Chaboche, J.L. and Rousselier, G., 1983, “On the Plastic and Viscoplastic Constitutive Equations – Part II: Application of Internal Variable Concepts to the 316 Stainless Steel,” Journal of Pressure Vessel Technology, Vol. 105, pp.159-164.

Chaboche, J.L., 1989, “Constitutive Equations for Cyclic Plasticity and Cyclic Viscoplasticity,” Int. J. Plasticity, Vol. 5 pp.247-302.

Chaboche, J.L., 1991, “On Some Modifications of Kinematic Hardening to Improve the Description of Ratcheting Effects,” Int. J. of Plasticity, Vol. 7, pp.661-678.

Chaboche, J.L. and Jung, O., 1998, “Application of a Kinemativ Hardening Viscoplasticity Model with Thresholds to the Residual Stress Relaxation,” Int. J. Plasticity, Vol. 13, pp.785-807.

Furukawa, T., Sugata, T., Yoshimura, S., and Hoffman, M., 2001, “An Automated System for Simulation and Parameter Identification of Inelastic C9nstitutive Models,” Int. J. of Computational Methods in Applied Mechanics and Engineering.

Furukawa, T. and Yagawa, G., 1997, “Inelastic Constitutive Parameter Identification Using an Evolutionary Algorithm with Continuous Individuals,” Int. J. Numerical Methods in Engineering, Vol. 40, pp.1071-1090.

Furukawa, T., and Hoffman, M., 2004, “Inelastic Finite Element Analysis Using Implicit Material Model,” Computational Mechnics, WCCM VI in Conjunction with APCOM’04.

Koo, G.H., Lee, H.Y., Joo, Y.S., et.al, 1999, “Thermal Stress Analysis and Service Limit Check for KALIMER Reactor Internal Structures,” Proceedings of the Korean Nuclear Society Spring Meeting.

Mroz, Z., 1967, “On the Description of Anisotropic Work hardening,” J. of the Mechanics and Physics of Solids, Vol. 15, pp.163-175.

Ohno, N and Wang, J.D., 1993, “Kinematic Hardening Rules with Critical State of Dynamic Recovery, Part I: Formulations and Basic Features for Ratcheting Behavior,” Int. J. of Plasticity, Vol. 9 pp.375-390.

Preger, W., 1956, “ A New Method of Analyzing Stresses and Strains in Work Hardening Plastic Solids,” J. of Applied Mechanics, Vol. 23, pp.493-496.

Puso, M., 2000, A Users Manual for the Nonlinear Kinematic Hardening Model for Cyclic Loading, Lawrence Livermore National Laboratory, UCRL-MA-140587.

Severud, L.K., 1991, “Creep-Fatigue Assessment Methods Using Elastic Analysis Results and Adjustments,” Transactions of the ASME, Vol.113, pp.34-40.

BIBLIOGRAPHIC INFORMATION SHEET			
Performing Org. Report No.	**Sponsoring Org. Report No.**	**Standard Report No.**	**INIS Subject Code**
KAERI/TR-3177/2006			

Title / Subtitle

Development of PARA-ID Code to Simulate Inelastic Constitutive Equations and Their Parameter Identifications for the Next Generation Reactor Designs

Project Manager and Dept. (Main Author)	Gyeong-Hoi Koo / Development of LMR Design Technology

Researcher and Dept.

J.H. Lee / Development of LMR Design Technology

Pub. Place	Taejon, Korea	**Pub. Org.**	KAERI	**Pub. Date**	March, 2006
Page	64P	**Fig. and Tab.**	Yes(o), No( )	**Size**	26 cm
Note					
Classified	Open(o), Outside( ), __Class		**Report Type**		
Sponsoring Org.			**Contract No.**		

Abstract (About 300 Words)

The establishment of the inelastic analysis technology is essential issue for a development of the next generation reactors subjected to elevated temperature operations. In this report, the peer investigation of constitutive equations in points of a ratcheting and creep-fatigue analysis is carried out and the methods extracting the constitutive parameters from experimental data are established. To perform simulations for each constitutive model, the PARA-ID (PARAmeter-IDentification) computer program is developed. By using this code, various simulations related with the parameter identification of the constitutive models are carried out.

Subject Keywords (About 10 Words)

PARA-ID Code, Inelastic Constitutive Equation, Parameter Identification, Next Generation Reactor, Structural Integrity Evaluation, Inelastic Strain, Ratcheting, Creep-Fatigue, Backstress, Material Hardening

서 지 정 보 양 식

수행기관 보고서번호	위탁기관 보고서번호	표준보고서번호	INIS 주제코드
KAERI/TR-3177/2006			

제목 /부제

차세대 원자로개발을 위한
비탄성 구성방정식 Simulation 및 재료상수 추출을 위한 PARA-ID 코드 개발

연구책임자 및 부서명 (TR 일 경우 주저자)	구 경 회 / 액체금속로 설계기술개발

연구자 및 부서명

이재한/ 액체금속로 설계기술개발

발 행 지	한국, 대전	**발행기관**	한국원자력(연)	**발행일**	2006. 3
페 이 지	64 P	**도 표**	유(o), 무( )	**크 기**	26 cm
참고사항					
비밀여부	공개 (o), 대외비( ), __급비밀		**보 고 서 종 류**		
연구위탁기관			**계 약 번 호**		

초록 (300 단어 내외)

차세대 원자로 설계를 위해서는 고온 비탄성해석 기술의 확보가 필수적이다. 본 보고서에서는 주어진 설계재료에 대한 라체칭, 크립-피로손상 해석에 필수적인 비탄성 구성방정식을 개발하기 위하여 지금까지 개발된 구성식 들의 특성을 검토하고 이들 구성식에 들어가는 재료상수들을 결정하기 위한 방법론을 확립하였다. 이를 위하여 각 구성방정식에 대한 Simulation 코드인 PARA-ID (PARAmeter-IDentification) 프로그램을 개발하고 이로부터 각 구성식에 요구되는 재료상수를 결정할 수 있는 절차를 정립하였다.

주제명 키워드 (10 단어 내외)

PARA-ID 코드, 비탄성구성식, 재료상수규명, 차세대원자로, 구조건전성평가, 비탄성변형률, 라체팅, 크립-피로, 재료경화